C.P. No. 653

C.P. No. 653

MINISTRY OF AVIATION

AERONAUTICAL RESEARCH COUNCIL

CURRENT PAPERS

Flight Measurements of the Dutch Roll Characteristics of a 60 Degree Delta Wing Aircraft (Fairey Delta 2) at Mach Numbers from 0.4 to 1.5 with Stability Derivatives Extracted by Vector Analysis

by

R. Rose, M.Sc.

LONDON: HER MAJESTY'S STATIONERY OFFICE

1963

NINE SHILLINGS NET

U.D.C. No. 533.652.1:533.693.3:533.6.011.3/5:533.6.053
533.6.013.16:533.6.013.413:533.6.08

C.P. No. 653
March, 1961

FLIGHT MEASUREMENTS OF THE DUTCH ROLL CHARACTERISTICS OF A 60 DEGREE DELTA WING AIRCRAFT (FAIREY DELTA 2) AT MACH NUMBERS FROM 0.4 TO 1.5 WITH STABILITY DERIVATIVES EXTRACTED BY VECTOR ANALYSIS

by

R. Rose, M.Sc.

SUMMARY

Lateral stability tests have been made on the Fairey Delta 2 research aircraft, studying the aircraft response following a rudder pulse. A description is given of the instrumentation used, and instrument response characteristics are discussed. Records of the damped Dutch roll oscillation (which persists after the initial pulse stage) have been analysed by the time vector method. The sideslip derivatives n_v, ℓ_v and y_v, and the damping derivatives n_r and ℓ_p have been extracted using estimated values of the relatively unimportant cross derivatives n_p and ℓ_r, which, due to the limitations of the instruments used, could not be extracted from the flight records. Values of the sideslip derivatives deduced from approximate formulae have been found to be in good agreement with the results from the time vector analysis for the range of flight conditions investigated.

Replaces R.A.E. Tech. Note No. Aero. 2752 - A.R.C.23,046.

LIST OF CONTENTS

LIST OF APPENDICES

LIST OF ILLUSTRATIONS

LIST OF ILLUSTRATIONS (Contd)

1 INTRODUCTION

The Fairey Delta 2 (ER 103) is a research aircraft built to investigate the characteristics of a 60 degree delta wing planform throughout a wide range of lift coefficient and Mach number. The flight tests have been programmed to investigate all aspects of aircraft stability, control and performance as accurately as possible, so that comparisons can be made with theory, wind tunnel, and free flight model tests.

The present note deals with that part of the flight programme devoted to the measurement of the principal lateral stability data. The limited flight endurance of a high performance aircraft like the Fairey Delta 2, requires the utmost economy in the conduct of flight tests. Thus lengthy procedures such as the recording of forced oscillations or measurements in steady asymmetric flight conditions can only be justified if more concise test techniques fail to yield the desired information. Furthermore, due to the reheat characteristics, it is not possible to stabilise speed on this aircraft in supersonic flight. A more convenient method, which is economical in flight test time, is the recording of the transient response of the aircraft following a rudder pulse. Potentially, an analysis of all modes of this motion, by the frequency response method, can yield all the lateral stability derivatives and also the rudder derivatives. However, experience so far has shown that the instrumentation available to date is inadequate in practice to realize this theoretical potential[1].

A rudder pulse generally excites all three lateral modes. However, shortly after the pulse has ceased, in practice only one damped oscillatory mode, conventionally called the Dutch roll oscillation, is found to persist. If this oscillation only is analysed using the time vector method, both extreme economy in computational effort and a clear understanding of the accuracy of the derived data are achieved. It is shown, however, that a fundamental limitation exists in this type of analysis. It is only possible to extract two derivatives for each degree of freedom, and thus only six derivatives in all may be found.

Certain approximate theoretical formulae for n_v and ℓ_v are considered in comparison with the corresponding values extracted by the vector method.

2 DESCRIPTION OF AIRCRAFT

The Fairey Delta 2 (ER 103) is a tailless research aircraft with a 60 degree delta wing of thickness chord ratio 0.04. Fig.1 shows a general arrangement of the aircraft, and Table 1 gives the principal dimensions. The aerodynamic controls are conventional elevator, aileron and rudder; all controls are operated by fully powered, irreversible duplicated hydraulic jacks. Feel for all three controls is provided by simple spring systems. The aircraft is powered by a Rolls Royce Avon RA 28 engine with a two position reheat nozzle. Fig.2 shows the aircraft tested, WG 777. In the tests made, the take-off weight of the aircraft was 13,884 lb and the maximum fuel load was 2,500 lb. The centre of gravity during the tests was nominally at 54.4% of the centre line chord, but due to fuel variations the actual centre of gravity position varied within the range of ±0.13% of this value.

3 DESCRIPTION OF INSTRUMENTATION AND GROUND CALIBRATIONS

The following parameters, relevant to the tests, were recorded:

Rate of roll

Rate of yaw

Lateral acceleration

Sideslip angle

Rudder angle

Aileron angle.

The transducers used to detect these parameters were:

(a) Accelerometer type IT.3-3-1, range ±0.4 'g',

(b) Ferranti rate gyro type IT.3-6-15, for rate of roll range ±30 degrees per second and for rate of yaw range ±15 degrees per second,

(c) Wind vane mounted on the nose boom of the aircraft range ±5 degrees.

(d) Control angles by potentiometer, rudder angle range ±7½ degrees, aileron angle range ±5 degrees.

The response characteristics of the instruments are important in dynamic flight testing and a brief description of the relevant features of the instruments is as follows:

The IT.3-3-1 accelerometer depends basically on a mass restrained by two cantilever springs; the position of the mass is determined by a potentiometer, and eddy current damping is provided by a copper shell moving in a permanent magnet. Since the damping provided by the eddy current is strictly proportional to velocity, the accelerometer will have acceptable dynamic characteristics if the friction between the potentiometer and brush is small. The accelerometer used was calibrated dynamically[2] for two levels of input, and linear results were obtained, (Fig.3). This design of accelerometer should not be subject to cross effects due to accelerations along other axes. As furthermore the majority of the flight tests were made in nominally 1 'g' level flight conditions, no calibrations were performed to determine such cross effects.

In the type IT.3-6-15 rate gyros, the damping is provided by a piston moving in silicone oil and the position of the gyroscope is determined by a potentiometer. The damping provided by this type of system is less satisfactory than eddy current damping, because (a) there is a variation of damping due to the effect of temperature on the viscosity of the oil, and (b) the dashpot does not produce strictly viscous damping, and as a result, the phase lag of one of the gyros varied significantly with the amplitude of input. However, it was established that the temperature in the instrumentation bay remained almost constant during the tests, and thus the first effect was unimportant. The two rate gyros were calibrated dynamically[2]. In each case the principal calibrations were made with an input amplitude corresponding roughly to the mean level of the range utilized during the flight tests. To check for linearity a few points were also obtained at a smaller amplitude of ±5 degrees per second. The measured phase lags of the two instruments are plotted in Figs.4 and 5. It can be seen that within the range tested, the rate of yaw gyro gave consistent results, whereas there is a marked dependence on amplitude of the response of the rate of roll gyro.

Considerable unserviceability was experienced in flight due to wear occurring over the central portion of the potentiometers. The wear was reduced to a minimum by removing the rate gyros from the aircraft when not required for the lateral stability tests and arranging that the gyros were

only running during the test period of any flight. In spite of these precautions, the rate gyros become unserviceable after only a few flights and this frequently delayed the flight programme. The reason for the potentiometer wear has not been definitely established, but laboratory tests indicated that it may well have been caused by increased friction due to variation in the deflection of the wiper arm with temperature and humidity; the increased friction would have the further effect of changing the dynamic response of the instrument.

Four wind vanes were mounted on the nose boom of the aircraft behind the pitot-static head. The vanes were arranged in a cruciform configuration so that two measured incidence and two measured sideslip. This preserved the symmetrical arrangement required to avoid errors in the transonic and supersonic speed range. The flight records showed that the wind vane did not provide a satisfactory means of measuring sideslip angle. Apparently friction at the bearings and between the potentiometer and brush caused unpredictable phase lags. Also deflection of the nose boom support under aerodynamic loads at high dynamic pressures introduced errors which could not be established by ground calibrations. In the detailed analysis of the flight records the wind vane readings have therefore been ignored. However the sideslip angle was deduced accurately and reliably from the lateral accelerometer readings.

The instrumentation used was the best available at the time the flight tests were made. One comment that should be made, however,is that all the transducers used a potentiometer pick-off. It is now generally realized that the friction inevitably associated with this type of pick-off leads to unsatisfactory dynamic instrument response. In future tests the rate gyros and the accelerometer will be replaced by transducers with A.C. pick-offs so that it is hoped to avoid these difficulties.

All the control angles, rates of roll and yaw, the sideslip angle and the lateral acceleration, were recorded on Hussenot recorders running at one inch per second paper speed. Pitot and static pressure were fed from a Mk.9h head mounted on the nose boom of the aircraft to both the pilots' instruments and the instrumentation. Indicated airspeed and altitude were recorded by standard instruments on the automatic observer. All recording equipment was installed in a bay above the nose wheel of the aircraft. The temperature in this bay was measured on a typical flight up to 40,000 ft altitude and was found to remain fairly constant between 10°C and 15°C.

4 FLIGHT TESTS

The flight tests were made at two altitudes, 10,000 ft and 40,000 ft; the range of speed covered was from M = 0.4 to 0.7 together with a few points at a Mach number of approximately 1.0 at 10,000 ft, and throughout the range from M = 0.7 to 1.5 at 40,000 ft. Most of the tests were made in 1 'g' level flight conditions but a few results were obtained at 40,000 ft in level turns, with a normal acceleration of 2 'g'.

The pilot used different test techniques at subsonic, transonic and supersonic speeds. Below a Mach number of 0.9, the airspeed and altitude were stabilised, and the aircraft trimmed longitudinally and laterally and then flown "hands off". After the recorders had been switched on, a sharp kick was given to the rudder pedals and the rudder allowed to return to its trim position under the action of the spring feel units. During the ensuing Dutch roll oscillation of the aircraft, the feet were kept off the rudder pedals. This procedure was adopted to ensure that no inadvertent aileron or rudder control inputs were made during the free oscillation. The recording was continued until the oscillation had decayed to a small magnitude or until the pilot required to regain control. A typical record is shown in Fig.6. Due to small asymmetries in the lateral trim of the aircraft the mean value

of the sideslip angle is not strictly zero. At transonic speeds the test procedure was generally similar except that it was not possible to fly the aircraft hands off due to lateral trim changes. This obviously increased the risk of accidental control movements during the tests and therefore any flight records which showed measurable aileron movements during the free oscillation of the aircraft were discarded. Supersonic speeds in level flight could only be attained by the use of reheat; this implied that the aircraft was either accelerating with reheat on, or decelerating with reheat off, and thus it was not possible to test under speed stabilised and trimmed conditions. As the attention of the pilot was concentrated on the engine instruments during reheat operation, all the tests were made during the decelerating part of the supersonic run when reheat was cancelled. It was not possible to fly the aircraft hands off due to difficulties in trimming in this speed range and again any records which showed detectable control inputs during the free oscillation were rejected.

The technique under 'g' at supersonic speeds was similar to that used in level flight except that the pilot attempted to trim the aircraft into a 2 'g' turn.

5 THE METHOD OF ANALYSIS

5.1 Introduction

Aircraft stability analysis is usually performed in stability axes (Fig.7). The origin O of the system is the aircraft centre of gravity. In this system of axes the X axis is fixed in the aircraft along the direction of the trimmed velocity vector. The Y axis is positive to starboard and normal to the plane of symmetry and the Z axis is positive downwards mutually perpendicular to the other two axes. Following a disturbance the velocities along the axes are u, v and w and the angular velocities of the axes are p, q and r.

The usual assumptions made in lateral stability analysis are:-

(a) disturbances are small and squares and products of small quantities may be ignored

(b) no coupling between longitudinal and lateral motions, thus $q = w = 0$ and u is constant and equal to V, the resultant velocity during any lateral disturbances.

For the flight test results to be considered here, the first assumption is valid. The second assumption is only justified provided there are no pitching moments due to sideslip and no marked effects of engine gyroscopic couples. Some coupling was recorded, but as this was only of small magnitude, and in view of the complication of the analysis and the limited accuracy of the instrumentation, its possible effects were ignored.

Making these assumptions, the number of independent variables is reduced to three, rolling, yawing and sideslip. However, in the tests, some rudder motion was recorded despite great care to avoid unwanted inputs by the pilot*; an allowance has been made for this in the analysis. Consideration of the stability equations shows that, when the aircraft is disturbed by a

---

* The rudder motion was not due to a failure of the rudder jack to operate irreversibly but was judged to be an aeroelastic effect due to fin distortion under sideslip loads. The rudder jack is at the base of the fin, and when the fin distorts under load the valves are parted and the jack operates. The geometry of the jack and operating rods is such that the rudder angle increases.

rudder pulse, the lateral modes which are excited are a heavily damped roll mode, a lightly damped or divergent spiral mode and a lightly damped oscillatory mode, conventionally called the Dutch roll oscillation.

The response of an aircraft to a rudder pulse is a function of the aerodynamic derivatives and the inertia characteristics of the aircraft and generally contains all the lateral modes. For the range of conditions explored in the present tests it was found that the response in sideslip was governed almost entirely by the Dutch roll mode only. The response in roll on the other hand contained elements of both the Dutch roll oscillation and the roll subsidence motion. The latter, however, was only prominent in the initial transient and after approximately one cycle of the recorded Dutch roll it had died down sufficiently for the remainder of the record to be interpreted as a pure lateral oscillation. The rate of yaw response, included both the Dutch roll mode and the spiral mode throughout the entire recorded period. It has been found possible to separate these two modes in the analysis by a graphical process which is discussed further in section 5.2.

Considering the complete aircraft motion recorded in response to a rudder pulse, theoretically all the lateral stability and rudder derivatives may be determined by a frequency response method of analysis or by solving the equations of motion in a sufficient number of distinct instances. However the standard of the instrumentation in the present tests was not adequate for reliable extraction of the minor derivatives n_p, ℓ_r and y_p. Using theoretical estimates for these derivatives (and for n_ζ, ℓ_ζ and y_ζ), the remaining derivatives can, however, be uniquely determined by considering the Dutch roll mode only. The time vector method has been chosen as the most suitable technique for analysing this oscillatory motion, although for comparison some approximate formulae are considered. It should be emphasised that the vector method is not an approximate procedure and the accuracy of the results should only be subject to,

(a) inaccuracies in the flight records, that is from instrumentation, recording and reading errors,

(b) errors in the assumed data, including the weight and moment of inertia and the assumed derivatives n_p, ℓ_r, y_p, n_ζ, ℓ_ζ and y_ζ.

A detailed analysis of the accuracy of the extracted stability derivatives would be difficult, but for an indication of the general level of accuracy, the effects of some systematic errors are considered in section 6.4.

In the analysis of the aircraft motions it is more usual to consider the disturbance velocity v in terms of the sideslip angle β, where by definition[3]

$$\sin \beta = \frac{v}{V}$$

and for small angles $\beta = \frac{v}{V}$.

Fig.8 shows the relation between β the angle of sideslip, ψ the angle of yaw and χ the flight path angle, all angles being shown positive. Although there are only four independent variables (p,r,β,ζ) to consider, a fifth dependent variable, the lateral acceleration, is of interest since this is easily measured.

The lateral acceleration of the aircraft centre of gravity normal to the flight path in trimmed level flight is

$$V\dot{\chi} = V(\dot{\psi} + \dot{\beta}) = V(r + \dot{\beta}) \tag{1}$$

since $$\dot{\psi} = r .$$

This is not however the acceleration recorded by a lateral accelerometer placed at the aircraft centre of gravity. The accelerometer measures, in the direction of the Y axis of the aircraft, a value

$$a_y = \frac{V}{g}(r + \dot{\beta}) - \phi . \tag{2}$$

The angle of bank ϕ, is related to the rate of roll p, by $p = \frac{d\phi}{dt}$.

The lateral equations of motion are:

$$L_\beta\beta + L_p p + L_r r + L_\zeta\zeta - A\dot{p} + E\dot{r} = 0 \tag{3}$$

$$N_\beta\beta + N_p p + N_r r + N_\zeta\zeta - C\dot{r} + E\dot{p} = 0 \tag{4}$$

$$Y_\beta\beta + Y_p p + Y_r r + Y_\zeta\zeta - m[V(r+\dot{\beta}) - g\phi] = 0 . \tag{5}$$

The sideforce equation may be written in terms of the acceleration a_y,

$$Y_\beta\beta + Y_p p + Y_r r + Y_\zeta\zeta - m\,a_y = 0 . \tag{6}$$

The necessary terms have been included in these equations to cover the inadvertent rudder movements which the records show to have occurred. For an oscillatory mode of oscillation, such as the exponentially damped Dutch roll oscillation following a rudder pulse, when the roll subsidence mode has disappeared and the spiral mode has been filtered, (as explained in section 5.2), the equations of motion may be written in the time vector notation of Appendix 2,

$$L_\beta\bar{\beta} + L_p\bar{p} + L_r\bar{r} + L_\zeta\bar{\zeta} - A\dot{\bar{p}} + E\dot{\bar{r}} = 0 \tag{7}$$

$$N_\beta\bar{\beta} + N_p\bar{p} + N_r\bar{r} + N_\zeta\bar{\zeta} - C\dot{\bar{r}} + E\dot{\bar{p}} = 0 \tag{8}$$

$$Y_\beta\bar{\beta} + Y_p\bar{p} + Y_r\bar{r} + Y_\zeta\bar{\zeta} - m\,\bar{a}_y = 0 . \tag{9}$$

In the equations, $\bar{\beta}$ for instance, represents the time vector of the sideslip angle β. Any one of these equations may be represented graphically by a vector polygon as explained in section 5.3. (Fig.15 shows a typical rolling moment polygon.)

The above equations apply only for trimmed level flight; in the case of a disturbance from trimmed banked flight, equation (2) must be modified to

$$a_y = \frac{V}{g}(r + \dot{\beta}) - \Delta\phi \cos \phi_o$$

where $\Delta\phi$ is the disturbance in bank

ϕ_o is the trimmed bank angle.

5.2 Method of reducing data to time vectors

The records have been analysed only after the initial rudder pulse has ceased and the roll mode has practically subsided. The spiral mode divergence is responsible for a distortion in the records of the Dutch roll oscillation which has been filtered out by a graphical method as follows.

The peaks of a decaying oscillation of the type shown in Fig.9 are plotted on a logarithmic graph paper as in Fig.10. The mean envelope of the oscillation is obtained from the locus of points such as B, where AB is equal to BC taking due account of the logarithmic scale (see Fig.10). This process is repeated for each independent variable and the best set of parallel lines drawn through the mean envelopes. The slope of these lines gives the damping of the oscillation. By subtracting the mean amplitude of the oscillation from the recorded variable (see Fig.9) the true datum line of the oscillation is obtained.

The time instants at which the oscillation crosses the datum line can be determined accurately, and by plotting these against number of cycles for each variable and drawing the best set of parallel straight lines the frequency, phase angles and amplitude ratios of the variables can be determined.

Applying instrument phase lag corrections then gives the true local values of these recorded quantities.

As explained in Appendix 1, the data are transformed to stability axes, and the lateral accelerometer readings corrected for the effects of rolling and yawing.

The sideslip angle may now be derived for the lateral acceleration at the aircraft centre of gravity. The kinematic relation of equation (2) may be written in the time vector notation as

$$\bar{a}_y = \frac{V}{g}(\dot{\bar{\beta}} + \bar{r}) - \bar{\phi} \quad . \tag{11}$$

From a knowledge of the time vectors $\bar{a}_y$, $\bar{r}$ and $\bar{\phi}$, $\dot{\bar{\beta}}$ may be determined* (see Fig.11). The time vector representing $\bar{\beta}$ then follows using the simple properties between time vector derivatives described in Appendix 2.

---

* In the case of banked flight the term ϕ must be replaced by $\Delta\phi \cos \phi_o$.

5.3 Extraction of stability derivatives by the time vector method

An example is given in Fig.12 of a set of the five vectors deduced from a typical Dutch roll oscillation. The accuracy of the phase angle of the rudder motion is considered to be poor and, ignoring minor scatter in the test data, it is assumed that the rudder angle is exactly in counterphase with the sideslip angle.

As explained in Ref.4, in this type of vector analysis only the relative phase angles and amplitude ratios of the vectors with respect to one another are of importance, and thus the time vectors are considered as invariant with respect to each other.

The data are now in a form suitable for the solution of the lateral equations of motion (7), (8) and (9), for the rolling, yawing, and sideways degrees of freedom respectively. These equations state that the sum of the vectors representing forces or moments acting on the aircraft during the oscillation are zero, consequently they must form a closed polygon. Any one of the vectors in the polygon is the product of a scalar with a vector of known magnitude and direction representing one of the recorded variables, for example, the rate of roll. The scalar quantity is either a moment or product of inertia* or an aerodynamic derivative. Three aerodynamic derivatives and one rudder control derivative, which is assumed to be known**, are associated with each vector polygon. It is obviously possible to solve for two stability derivatives, in each degree of freedom, provided the third derivative and the rudder derivative are known from another source. Six derivatives in all may be extracted since these are three degrees of freedom. The three derivatives which play the least important part in the Dutch roll oscillation are n_p, ℓ_r and y_p. Theoretical values of n_p, ℓ_r, n_ζ, ℓ_ζ and y_ζ have been assumed and are shown in Figs.13 and 14; y_p is a minor derivative which is difficult to estimate accurately and it is assumed to be negligible.

Fig.15 shows a typical rolling moment vector polygon. Using the estimated values of ℓ_r and ℓ_ζ, the stability derivatives ℓ_v and ℓ_p can be determined from the side lengths established by closing the polygon.

Fig.16 shows a typical yawing moment vector polygon; in this case estimated values of n_p and n_ζ are used to extract the derivatives n_v and n_r. For the case illustrated, the cross derivative n_p is generally considered to be the least important in the Dutch roll oscillation, but unfortunately at high supersonic speed this may not necessarily be true. Nevertheless a theoretical estimate was accepted for this derivative and n_r was extracted.

A typical sideforce vector polygon is shown in Fig.17. Since y_p is assumed to be zero, the derivatives y_v and y_r are determined uniquely. However, since y_r is a minor term and difficult to extract accurately, values of this derivative are not recorded here.

---

* Estimates of the moments and products of inertia were supplied by the Fairey Aviation Co. and values are given in Table 1. They are now being measured on a specially designed ground rig.

** Estimates of rudder derivatives were also supplied by the Fairey Aviation Co., and an allowance made for the effect of Mach number. The values used are shown in Fig.13.

There are several advantages to be gained from the use of the time vector method of analysis. In the first place a good physical insight is gained of the motion of the aircraft during the Dutch roll oscillation. Also the sensitivity of the extracted derivative to the accuracy of the recorded data can be assessed directly, and the effect of systematic errors due to incorrectly assumed values of the moments of inertia and aerodynamic derivatives can be shown in a straight-forward way. The level of accuracy is considered further in section 6.4. In addition, the corrections due to inadvertent rudder movements are easily applied.

5.4 Stability derivatives deduced from simple formulae based on approximate analysis

Ref.5 gives two approximate formulae for the period and roll to yaw ratio of the Dutch roll oscillation; these approximations neglect all but the sideslip derivatives. They can be solved to give:

$$n_v = \frac{i_C}{\mu_2} J_1^2 \frac{\left[1 + \frac{\bar{p}}{\bar{r}} \frac{i_E}{i_C}\right]}{\left[1 + \frac{i_E^2}{i_A i_C}\right]} \qquad (12)$$

$$\mathcal{L}_v = -\frac{i_A}{\mu_2} J_1^2 \frac{\left[\frac{\bar{p}}{\bar{r}} + \frac{i_E}{i_A}\right]}{\left[1 + \frac{i_E^2}{i_A i_C}\right]} . \qquad (13)$$

6 RESULTS AND DISCUSSION

The results obtained from the analysis of the Dutch roll oscillations are shown in Figs.18 to 34. Figs.18 to 27 give fundamental data in frequency, damping, amplitude ratios and phase angles between the variables. The lateral stability derivatives derived from these results by the time vector method are shown in Figs.28, 30, 32, 33 and 34. Also the yawing and rolling moment derivatives due to sideslip, obtained from the simple approximate method, are shown in Figs.29 and 31. Most of the data were obtained in level flight at 40,000 ft, but some results were obtained at 40,000 ft pulling at 1 'g' excess normal acceleration and some in level flight at 10,000 ft. These additional results indicate that there are noticeable effects of incidence and aeroelasticity without, however, allowing them to be separated out.

6.1 Characteristics of the Dutch roll oscillation

Fig.18 shows the more important characteristics of the Dutch roll oscillation; namely the damping, period, and roll to yaw ratio for the aircraft in level flight at 40,000 ft. The general level of damping is very low, the damping ratio being constant at 0.07 up to M = 0.9 and rising very slightly to a maximum at M = 0.98 before falling quite rapidly to 0.04 at M = 1.2. Thereafter it increases slightly up to M = 1.5. The period of the Dutch roll oscillation decreases from 3 seconds at M = 0.7 to 2 seconds at M = 1.0 and then decreases to 1.7 seconds at M = 1.2 and then remains roughly constant. The roll to yaw ratio is about 4 at all speeds.

It is interesting to note the pilots' impressions of flying the aircraft. At subsonic speeds up to M = 0.9, the aircraft is lightly damped and requires constant attention from the pilot. At transonic speeds between M = 0.9 to 1.05, the aircraft is difficult to trim laterally and is very difficult to fly, the pilot having the impression of the aircraft being in a continuous Dutch roll oscillation. At supersonic speeds, the trim changes are reduced and the aircraft becomes more pleasant to fly.

These impressions are contrary in important respects to those one would deduce from Fig.18 where it is seen that at transonic speeds, the damping of the Dutch roll is at a maximum and at supersonic speeds at its minimum. In fact, the pilots' impressions of poor flying qualities at transonic speeds are due to the difficulty in trimming the aircraft. The trimming difficulties are caused by the controls being very effective at these speeds and also by the backlash between the stick and ailerons. Repeated lateral retrimming of the aircraft is required, and small associated control inputs are continuously exciting the Dutch roll oscillation.

Fig.19 shows the ratio of the rudder angle movement to sideslip angle caused apparently by the elastic distortion (see footnote in section 5.1) of the fin and rudder during the Dutch roll oscillation. The motion of the rudder is in counterphase with the sideslip angle and in the sense to increase the effectiveness of the fin. With this phase relationship the rudder motion does not affect the damping of the Dutch roll oscillation. Since the rudder motion depends on fin loads, it is a function of the equivalent airspeed V_i and Mach number. In Fig.20 the ratio of rudder angle to sideslip angle has been divided by V_i^2. The scatter of the results is large because the greatest rudder angle movement recorded was about $\pm\frac{1}{4}$ degree whilst the total range of measurement was $\pm 7\frac{1}{2}$ degrees. Nevertheless this rudder motion is important since it increased the apparent directional stability n_v by about 5%.

6.2 Relationship of the phase and magnitude of parameters of the Dutch roll oscillation

The quantities discussed in this section are not directly significant as flying quality criteria but they are significant for the further analysis of the data as they express properties of the Dutch roll motion which are utilized in the extraction of the derivatives.

Fig.21 shows the non-dimensional frequency parameter J_1; since this parameter depends fundamentally upon the period of the motion the accuracy is good and there is very little scatter. J_1 is mainly a function of the directional stability derivative n_v. Increase of lift coefficient has a small effect at 40,000 ft.

The non-dimensional damping factor R_1 is shown in Fig.22. This parameter is more difficult to measure accurately; however in the present tests the scatter is not large. A large effect of incidence at 40,000 ft is apparent; this is partly caused by an increased contribution of the product of inertia to the damping and partly by the increase of the damping in yaw derivative n_r.

Fig.23 shows the ratio of rolling velocity to lateral acceleration.

The scatter of ε_{rp}, the phase angle between rolling and yawing velocities, (Fig.24) is quite small. It is largest at transonic speeds where it is about $\pm 8^\circ$. At other speeds it is about $\pm 4^\circ$ which probably represents the reading accuracy of a Hussenot record.

Similar remarks apply for $\varepsilon_{a_y p}$, the phase angle between the lateral acceleration and the rate of roll, (Fig.25).

Fig.26 shows $\varepsilon_{\beta r}$ the phase angle between the sideslip angle and the yawing velocity. The scatter for this phase angle is very small. This quantity is derived from equation (11) and it can be seen from Fig.11 that it is almost proportional to the amplitude of the lateral acceleration a_y. In consequence its determination is not dependent on the measurement of a phase angle from a flight record.

The phase angle between the sideslip angle and the lateral acceleration, $\varepsilon_{\beta a_y}$, is shown in Fig.27. The same remarks apply as for the scatter of $\varepsilon_{\beta r}$.

6.3 The derivatives extracted from the flight data

The stability derivatives depend on Mach number, incidence, and also aeroelastic distortion effects. It is not practical in the flight tests to separate uniquely these effects. For instance, comparison of results at a given Mach number in level flight at two altitudes involves a change of equivalent airspeed which alters the lift coefficient as well as the aeroelastic effects. Also comparison of results at a given Mach number at a fixed altitude for different values of normal acceleration, gives a change of lift coefficient, but the increased loading involves some aeroelastic distortion.

In the following subsections, the results for the sideslip derivatives n_v, ℓ_v and y_v and the damping derivatives ℓ_p and n_r, are considered.

6.3.1 Yawing moment due to sideslip n_v

Fig.28 shows the variation with Mach number of the stability derivatives n_v, deduced by the vector method. In level flight at 40,000 ft, n_v increases from 0.075 at subsonic speeds to a maximum of 0.108 at M = 1.05 and thereafter falls gradually to 0.08 at M = 1.45. The few points at 40,000 ft at 1 'g' excess normal acceleration indicate that n_v is reduced due presumably to the effect of increased incidence.

Fig.29 shows comparable values deduced by the approximate method and also shown in the same figure are corresponding results deduced by the vector method. The agreement between the approximation and the vector method is very good. However the remarks of section 6.3 regarding the validity of the simple approximation under different conditions should be noted.

6.3.2 Rolling moment due to sideslip ℓ_v

Fig.30 shows the variation of ℓ_v with Mach number, as obtained from analysis by the vector method. The level flight results at 40,000 ft show a gradual decrease except for a sudden increase between M = 0.9 to M = 1.0 due to Mach number effect. The gradual decrease in $-\ell_v$ in steady level flight as Mach number increases is caused by the reduction of lift coefficient since $-\ell_v$ is a function of C_L. The other results at 40,000 ft at 1 'g' excess normal acceleration and in level flight at 10,000 ft show similar trends and also reflect the effect of the change in lift coefficient.

Fig.31 shows the variation with Mach number of the value of ℓ_v given by the approximate method, compared with the corresponding results from the vector method. The agreement between the two methods is reasonable, the approximate method tending to underestimate $-\ell_v$ by about 20%.

6.3.3 Sideforce due to sideslip y_v

Fig.32 shows the variation with Mach number of the sideforce derivative y_v. The results show a gradual increase of $-y_v$ with Mach number up to M = 1.00 followed by a gradual decrease. The effect of increased incidence at 40,000 ft is to increase $-y_v$ slightly; at 10,000 ft a small reduction in $-y_v$ occurs at transonic speeds presumably due to aeroelastic effects in the fin. The general trend of the results is reflected by the variation of the fin lift curve slope with Mach number.

6.3.4 Rolling moment due to rolling velocity ℓ_p

Fig.33 shows the variation of the damping in roll derivative, ℓ_p, with Mach number. The value of $-\ell_p$ in level flight at 40,000 ft is constant at subsonic speeds and shows a small increase at transonic speeds and then falls gradually away at supersonic speeds to about the same value as at subsonic speeds. The effect of increased incidence at 40,000 ft is most marked and $-\ell_p$ is increased at all speeds below M = 1.5. The level flight results at 10,000 ft show a small reduction in $-\ell_p$ probably due to aeroelastic effects.

6.3.5 Yawing moment due to yawing velocity n_r

Fig.34 shows the estimated variation with Mach number of the damping in yaw derivative, n_r. It must be emphasised that the value of n_r obtained by this analysis from a given set of flight data is dependent on the assumed value of n_p. Fig.14 shows the theoretically estimated value of n_p to be very small below a Mach number of 1.4, but above this speed large values are predicted, and it can be shown that they will have a significant effect on the deduced value of n_r. The flight results suggest that the assumed theoretical values of n_p above a Mach number of 1.4 must be treated with reserve as their use results in rather unexpected and unexplained variations in the computed value of n_r with both Mach number and lift coefficient. However as no better estimates of n_p are yet available the results of n_r given in Fig.39 must be accepted as the best approximation. In level flight

at 40,000 ft $-n_r$ is constant at subsonic speeds and increases rapidly at a Mach number of 1.0 and then falls at supersonic speeds to a somewhat lower value than at subsonic speeds. The effect of increased incidence at 40,000 ft is to increase $-n_r$ below M = 1.4 but to reduce $-n_r$ above this speed. In level flight at 10,000 ft there are large aeroelastic effects at transonic speeds and $-n_r$ is almost zero at a Mach number just below unity.

6.4 Assessment of the accuracy of the results

Several systematic errors exist in this type of analysis. These errors are caused by incorrectly estimated values of the moments and products of inertia, the cross derivatives and the rudder derivatives. From equations (7) and (8) and the corresponding rolling and yawing moment polygons of Figs. 15 and 16 it is seen that the extracted derivatives are directly proportional to the moments of inertia. Thus any errors in the estimates of the moments of inertia are reflected in similar errors in the derivatives. No detailed analysis of the effect of systematic errors is attempted in this section but some typical errors are evaluated for level flight conditions at 40,000 ft at a Mach number of 1.4. The inclination of the principal axis of inertia is very difficult to estimate, but an error of $\frac{1}{2}$ degree in the inclination of this axis results in an increase of 50% in the product of inertia for this flight condition. This gives a 12% increase in the damping in yaw derivative, n_r, and a 4% increase in the directional stability derivative; however, the remaining derivatives, ℓ_p and ℓ_v, are practically unaffected. Increasing the theoretically estimated value of ℓ_r by 50%, decreases the value of ℓ_p by 3% and ℓ_v by 0.8%. A decrease of 0.02 in the theoretical estimate of n_p increases n_r by 10% and decreases n_v by 4%. Increasing the estimated values of the rudder derivatives by 50%, ℓ_ζ and n_ζ, gives a small change of 0.4% in ℓ_v, a 2.4% increase in n_v but no changes in ℓ_p and n_r.

Although the above results only apply to the particular case considered, the magnitudes of the systematic errors are of the same order for most flight conditions. Thus it is seen that an error in the moments of inertia is reflected equally in all the extracted derivatives. However, in the case of the product of inertia, only the damping in yaw derivative, n_r, is affected significantly. Quite large errors in the theoretically estimated cross derivatives, n_p and ℓ_r, and the rudder derivatives, n_ζ and ℓ_ζ, have very small effects on the extracted derivatives.

In addition to the systematic errors, scatter of the extracted derivatives is caused by random errors of the reading of the recorded data.

7 CONCLUSIONS

From lateral stability tests using a rudder pulse method, the important Dutch roll characteristics, namely the damping ratio, period, and roll to yaw ratio have been obtained and are shown in Fig.21. The following stability derivatives have been extracted, n_v, ℓ_v, y_v, ℓ_p and n_r, the results being shown in Figs.28 to 34. All the derivatives are functions of Mach number; however the effects of lift coefficient and aeroelasticity are equally important. Approximate formulae have been used as a cross check on the values of n_v and ℓ_v.

The time vector method has been found particularly suitable for the analysis of the results and has the following advantages. A good physical insight is gained of the motion of the aircraft during the Dutch roll oscillation, and the effects of systematic errors due to the assumed values of the moments of inertia and aerodynamic derivatives can be considered (section 6.4). Furthermore, corrections due to instrument dynamic response and inadvertent rudder movements are easily applied.

Although the instrumentation used was the best available at the time the flight tests were made, it suffered from some limitations. All the transducers used a potentiometer pick-off. It is now generally realized that the friction inevitably associated with this type of pick-off leads to unsatisfactory dynamic instrument response. In future tests the rate gyros and the accelerometer will be replaced by transducers with A.C. pick-offs and it is hoped thereby to avoid these difficulties.

LIST OF SYMBOLS

Definition of axes and variables

$O\ X\ Y\ Z$	System of stability axes	
$O\ X_B\ Y_B\ Z_B$	System of body datum axes	
$O\ X_G\ Y_G\ Z_G$	System of rate gyro datum body axes	
$u,\ v,\ w,$	incremental velocities along the axes	Suffices B, G, denote the various reference systems
$p,\ q,\ r,$	angular velocities about the axes	
α	trim body datum incidence	
$\beta = \frac{v}{V}$	true angle of sideslip	
ϕ	angle of bank	
ψ	angle of yaw	

LIST OF SYMBOLS (Contd)

χ	angle of flight path relative to a fixed datum line
ζ	rudder angle
a_y	lateral acceleration at the aircraft centre of gravity
a_{y_i}	reading of a lateral accelerometer at some position other than the aircraft centre of gravity

Note: A dot above any of the above quantities denotes differentiation with respect to time.

A bar above any of the above quantities denotes a time vector.

Stability derivatives

$\ell_v = \frac{L_v}{\rho V S s} = \frac{L_\beta}{\rho V^2 S s}$, rolling moment due to sideslip derivative where $L_v = \frac{\partial L}{\partial v}$ etc.

$\ell_p = \frac{L_p}{\rho V S s^2}$, rolling moment due to rolling velocity derivatives

$\ell_r = \frac{L_r}{\rho V S s^2}$, rolling moment due to yawing velocity derivative

$\ell_\zeta = \frac{L_\zeta}{\rho V^2 S s}$, rolling moment due to rudder derivative

$n_v = \frac{N_v}{\rho V S s} = \frac{N_\beta}{\rho V^2 S s}$, yawing moment due to sideslip derivative

$n_p = \frac{N_p}{\rho V S s^2}$, yawing moment due to rolling velocity derivative

$n_r = \frac{N_r}{\rho V S s^2}$, yawing moment due to yawing velocity derivative

$n_\zeta = \frac{N_\zeta}{\rho V^2 S s}$, yawing moment due to rudder derivative

LIST OF SYMBOLS (Contd)

$y_v = \frac{Y_v}{\rho V S} = \frac{Y_\beta}{\rho V^2 S}$, sideforce due to sideslip derivative

$y_p = \frac{Y_p}{\rho V S s}$, sideforce due to rolling velocity derivative

$y_r = \frac{Y_r}{\rho V S s}$, sideforce due to yawing velocity derivative

$y_\zeta = \frac{Y_\zeta}{\rho V^2 S}$, sideforce due to rudder derivative

Dutch roll parameters

$\mathcal{J}_1 = \frac{2\pi}{P_1}$ circular frequency

$P_1 =$ Period

$\mathcal{J}_{1_o} = \mathcal{J}_1 / \sqrt{1 - \zeta_1^2}$, undamped circular frequency

$J_1 = \mathcal{J}_1 \hat{t}$ non dimensional circular frequency

$\mathcal{R}_1 =$ damping factor

$R_1 = \mathcal{R}_1 \hat{t}$ non dimensional damping factor

$\delta_1 = \mathcal{R}_1 P_1$ logarithmic decrement

$\zeta_1 =$ damping ratio

$\varepsilon_D = \tan^{-1}\left(\frac{\delta_1}{2\pi}\right)$, the damping angle

$\varepsilon_{rp} =$ phase angle by which rate of yaw leads rate of roll

$\varepsilon a_y p =$ phase angle by which lateral acceleration leads rate of roll

$\varepsilon_{\beta r} =$ phase angle by which sideslip angle leads rate of yaw

$\varepsilon_{\beta a_y} =$ phase angle by which sideslip angle leads lateral acceleration

Inertia characteristics

A = rolling moment of inertia, slugs ft^2

C = yawing moment of inertia, slugs ft^2

E = product of inertia, slugs ft^2

$i_A = \frac{A}{ms^2}$ rolling moment of inertia coefficient

$i_C = \frac{C}{ms^2}$ yawing moment of inertia coefficient

$i_E = \frac{E}{ms^2}$ product of inertia coefficient

General data

g acceleration due to gravity, ft/sec^2

m aircraft mass, slugs

S gross wing area, ft^2

s semispan, ft

$\hat{t} = \frac{m}{\rho S V}$, aerodynamic time, seconds

V true speed, ft/sec

V_i equivalent airspeed, knots

x_1, y_1, z_1 co-ordinates of lateral accelerometer relative to the aircraft centre of gravity in body datum axes

$\chi_1 = \alpha + \varepsilon_1$

ρ air density, slugs/ft^3

$\mu_2 = \frac{m}{\rho S s}$, relative aircraft density

LIST OF REFERENCES

No.	Author	Title, etc.
1	Cooper, A.H. Wener, N.L. Wilson, D.A.	Flight test determination of the stability and control derivatives for the F106A airplane. Convair Report ZC-8-559. (P.84891). August 1959.
2	Spavins, C.S. Dee, F.W.	Frequency response and cross effect calibrations of some rate gyros and accelerometers with specific reference to dynamic flight experiments. A.R.C.24,281 June,1962.
3	Warren, C.H.E.	Definition of the angles of incidence and of sideslip. A.R.C. C.P.124 August, 1952.
4	Doetsch, K.H.	The time vector method for stability investigations. A.R.C. R.&M. 2945 August, 1953.
5	Thomas, H.H.B.M. Neumark, S.	Interim note on the stability and response characteristics of supersonic aircraft. (Linear theory). A.R.C. 18,263 November, 1955.

ATTACHED:

Appendices 1 and 2
Table 1

APPENDIX 1

TRANSFORMATION OF RECORDED DATA TO STABILITY AXES

The rates of roll and yaw were measured by rate gyros about a system of datum axes which were not in general aligned with the stability axes appropriate to a given flight condition. The two systems of axes are shown in Fig.7. The angle between the X axes of the two systems is

$$\chi_1 = \alpha + \varepsilon_1 \tag{14}$$

where α is the trimmed body datum incidence and ε_1 is the angle between the rate gyro datum and body datum.

If the time vectors representing the rate of roll and yaw are defined as $\bar{p}_G$ and $\bar{r}_G$ about the rate gyro axes, and $\bar{p}$ and $\bar{r}$ about the stability axes, the transformation between the two systems of axes is given by

$$\bar{r} = \bar{r}_G \cos \chi_1 - \bar{p}_G \sin \chi_1 \tag{15}$$

$$\bar{p} = \bar{p}_G \cos \chi_1 + \bar{r}_G \sin \chi_1 \, . \tag{16}$$

This transformation is performed conveniently by the simple addition of time vectors as shown in Fig.35.

In addition, since it was not possible to place the lateral accelerometer at the aircraft centre of gravity, it is necessary to correct the lateral accelerometer reading for the effect of rolling and yawing of the aircraft. Fig.36 shows a system of body datum axes with the origin at the centre of gravity O, the co-ordinates of the position, C, of the accelerometer with respect to these axes being (x_1, y_1, z_1). If a_{y_i} is the reading of the lateral accelerometer and a_y the acceleration at the centre of gravity O (both positive to starboard) then

$$a_y = a_{y_i} - x_1 \dot{r}_B + z_1 \dot{p}_B + y_1 \left(p_B^2 + r_B^2 \right) . \tag{17}$$

For the conditions of the tests, the last term of equation is negligible as it represents the sum of squares of small quantities; also it is sufficiently accurate here to assume $p_G = p_B$ and $r_G = r_B$. Making these assumptions equation (17) may be written in terms of the appropriate time vectors as

$$\bar{a}_y = \bar{a}_{y_i} - x_1 \dot{\bar{r}}_G + z_1 \dot{\bar{p}}_G \tag{18}$$

and the transformations performed vectorially as described in Appendix 2 and shown in Fig.37.

APPENDIX 2

THE TIME VECTOR METHOD OF ANALYSING EXPONENTIALLY DAMPED SINUSOIDAL OSCILLATIONS

The equation of motion representing a simple mass and spring system with damping proportional to velocity is

$$\ddot{x} + 2\zeta \omega_n \dot{x} + \omega_n^2 x = 0 \qquad (19)$$

where ω_n is the undamped natural frequency when $\zeta = 0$, and ζ is the damping ratio.

The damped frequency ω of the oscillation is related to the undamped frequency by

$$\omega = \omega_n \sqrt{1 - \zeta^2} .$$

The general solution of equation (1) is

$$x = x_o e^{-\zeta \omega_n t} \sin \left[\omega_n \sqrt{1 - \zeta^2}\, t + \phi \right] \qquad (20)$$

where x_o and ϕ are arbitrary constants determined by the boundary conditions.

In the simple case of zero damping, equation (20) becomes

$$x = x_o \sin [\omega_n t + \phi] \qquad (21)$$

and the first derivatives of x with respect to time is

$$\dot{x} = x_o \omega_n \cos [\omega_n t + \phi] . \qquad (22)$$

The variation of x with time may be represented by a "time vector" $\bar{x}$ of constant length x_o which is rotating at constant angular velocity ω_n and starts from an angle ϕ at time zero, see Fig.38. The variation of $\dot{x}$ with time may be represented by another time vector $\dot{\bar{x}}$ of constant amplitude $x_o \omega_n$ rotating with angular velocity ω_n and advanced in phase by 90° relative to the time vector $\bar{x}$, see Fig.38. The two time vectors are time invariant with respect to each other.

So far we have only considered time vectors in the case of simple undamped oscillations, however the same concept may be applied to exponentially damped oscillations. The time derivative $\dot{x}$ of equation (20) is

$$\dot{x} = \omega_n x_o e^{-\zeta\omega_n t}\left[\sqrt{1-\zeta^2}\cos\left(\omega_n\sqrt{1-\zeta^2}\,t+\phi\right) - \zeta\sin\left(\omega_n\sqrt{1-\zeta^2}\,t+\phi\right)\right]$$

$$= \omega_n x_o e^{-\zeta\omega_n t}\left[\cos\varepsilon_D\cos\left(\omega t+\phi\right) - \sin\varepsilon_D\sin\left(\omega t+\phi\right)\right]$$

where

$$\varepsilon_D = \tan^{-1}\frac{\zeta}{\sqrt{1-\zeta^2}}\,.$$

Thus

$$\dot{x} = \omega_n x_o \ell^{-\zeta\omega_n t}\cos\left[\omega t + \phi + \varepsilon_D\right]\,. \qquad (23)$$

In the case of the damped oscillation both x and $\dot{x}$ may be represented by two time vectors $\bar{x}$ and $\dot{\bar{x}}$ which rotate at constant angular velocity ω. The magnitudes of $\bar{x}$ and $\dot{\bar{x}}$ at time zero are x_o and $x_o\omega_n$ respectively and both are shrinking at a rate of $\ell^{-\zeta\omega_n t}$ with time. In this case the phase of $\dot{\bar{x}}$ is $90^\circ + \varepsilon_D$ in advance of $\bar{x}$, where ε_D is called the damping angle. Again the two time vectors $\bar{x}$ and $\dot{\bar{x}}$ are time invariant with respect to each other, and are represented in Fig.39.

One of the most useful properties of a time vector has been established. Namely that if say the rate of roll is measured in an exponentially damped sinusoidal oscillation and is represented by a time vector $\bar{x}$ rotating at the frequency of the oscillation, then the time derivative of the rate of roll, i.e. the acceleration in roll, may be represented by another time vector of magnitude increased in the ratio of the undamped frequency and phase angle increased by 90° plus the damping angle. Also the integral of the rate of roll, the angle of bank, may be represented by another time vector, in this case the magnitude is reduced in ratio of the undamped frequency and the phase lag by 90° plus the damping angle.

Since time vectors are invariant with respect to each other they may be drawn as vectors which do not alter with time. If the magnitude and phase relation of between two or more time vectors is known, then the vector sum of any proportion of the vectors may be obtained easily as shown in Fig.40.

TABLE 1

Fairey Delta 2 - Principal dimensions and inertia characteristics

Wing

Gross area	360 sq ft
Span	26 ft 10 in.
Nominal centre line chord	25 ft
Tip chord	1 ft 10 in.
Mean aerodynamic chord	16 ft 9 in.
Wing section	4% symmetrical, max t/c at 29.5% C
Leading edge sweep back	59.92°
Trailing edge sweep back	0°
Twist	0°
Dihedral	0°
Wing-incidence with respect to fuselage datum	+1.5°

Weight and centre of gravity

All up weight at take-off	13,884 lb
Fuel contents	2,500 lb
Centre of gravity position at take-off, undercarriage down	163.9 in. aft of L.E. of centre-line chord

Inertia characteristics (Firm's estimates)

No fuel

Pitching moment of inertia	646,000 lb ft^2
Rolling moment of inertia	158,000 lb ft^2
Yawing moment of inertia	793,000 lb ft^2

Full fuel

Pitching moment of inertia	789,000 lb ft^2
Rolling moment of inertia	193,000 lb ft^2
Yawing moment of inertia	968,000 lb ft^2

Inertia ratios and principal axes inclination (full fuel or no fuel)

i_A	0.0775
i_B	0.204
i_C	0.389

Inclination of principal axes $1\frac{1}{2}^\circ$ nose down to body datum

WT.2078 C.P.653 K3 - Printed in England.

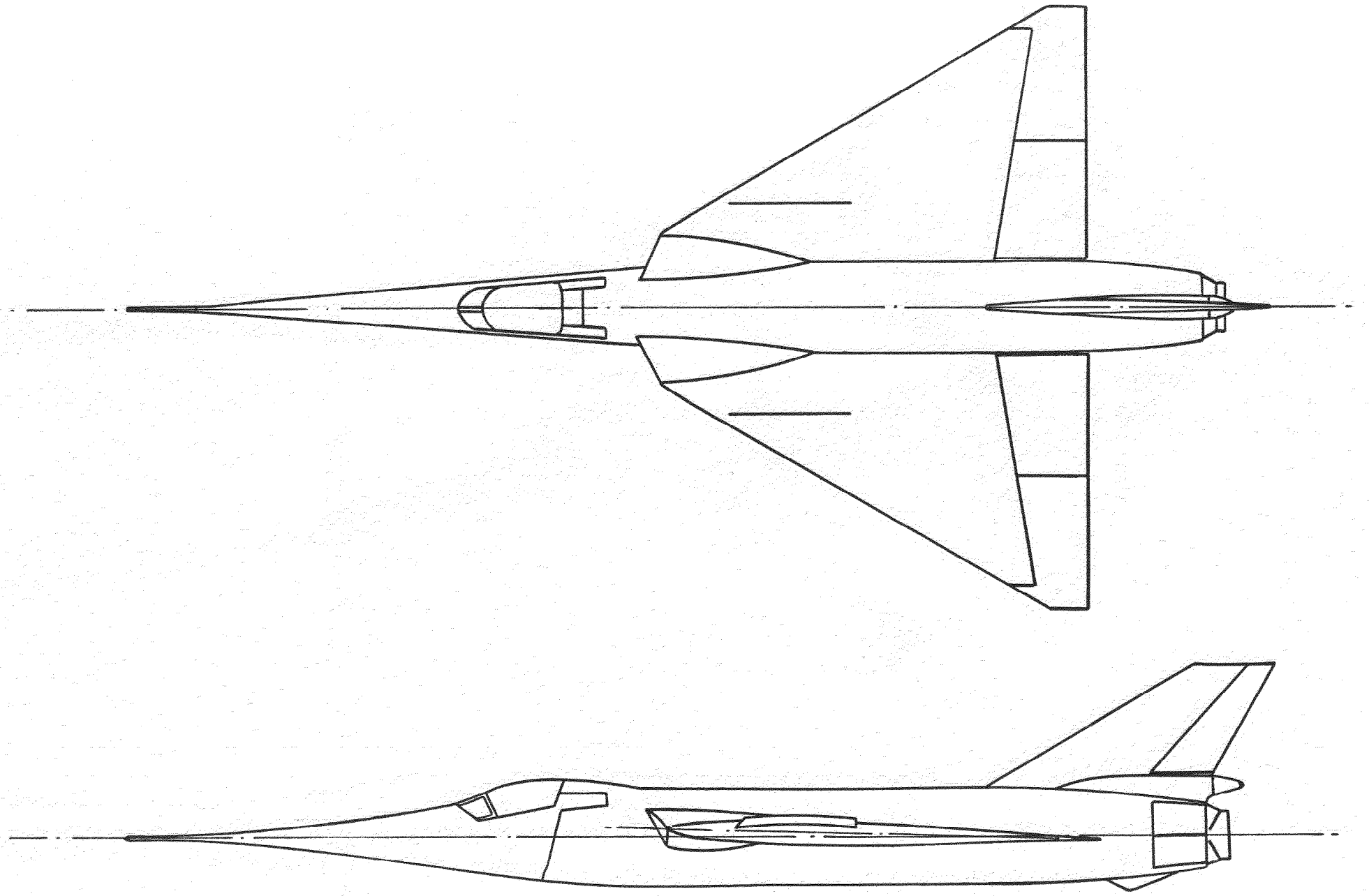

GURE I. GENERAL ARRANGEMENT OF THE FAIREY DELTA 2

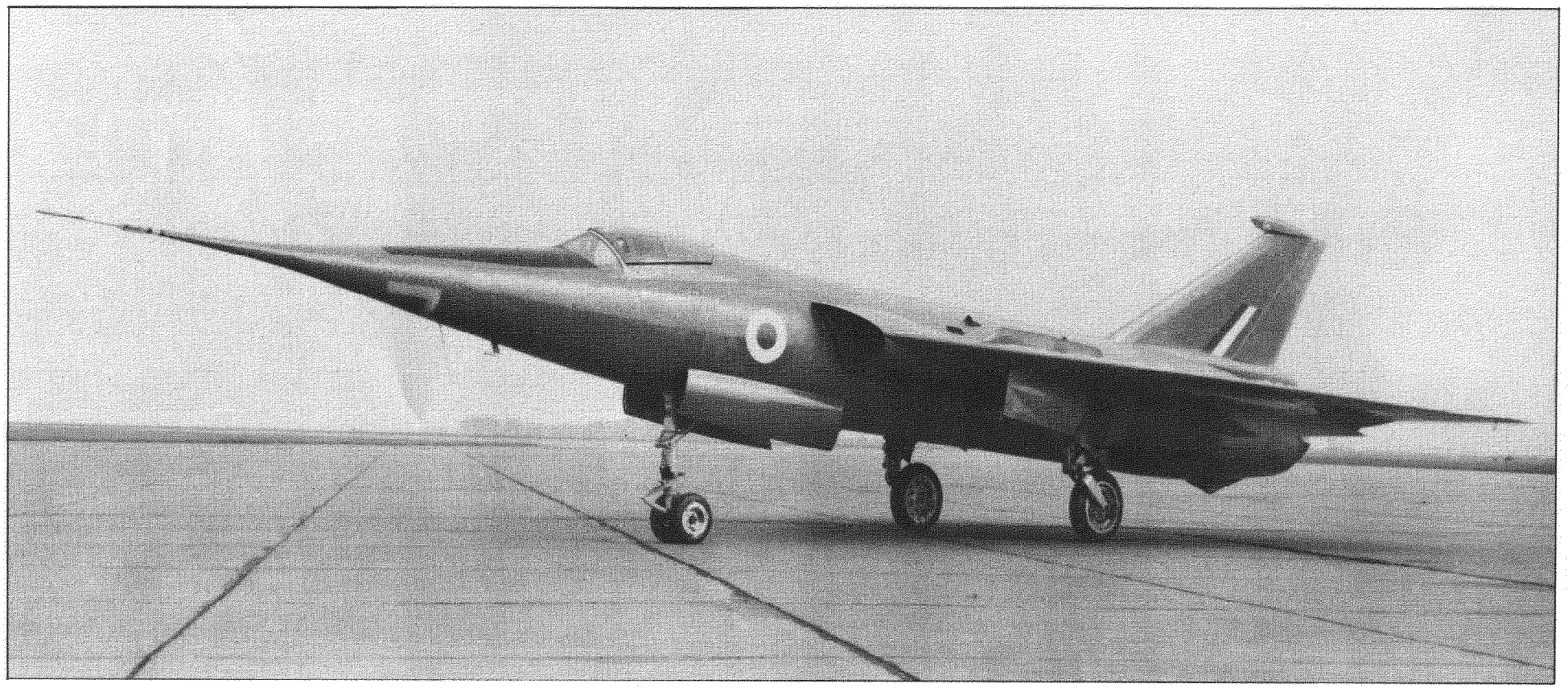

FIG.2. FAIREY DELTA 2

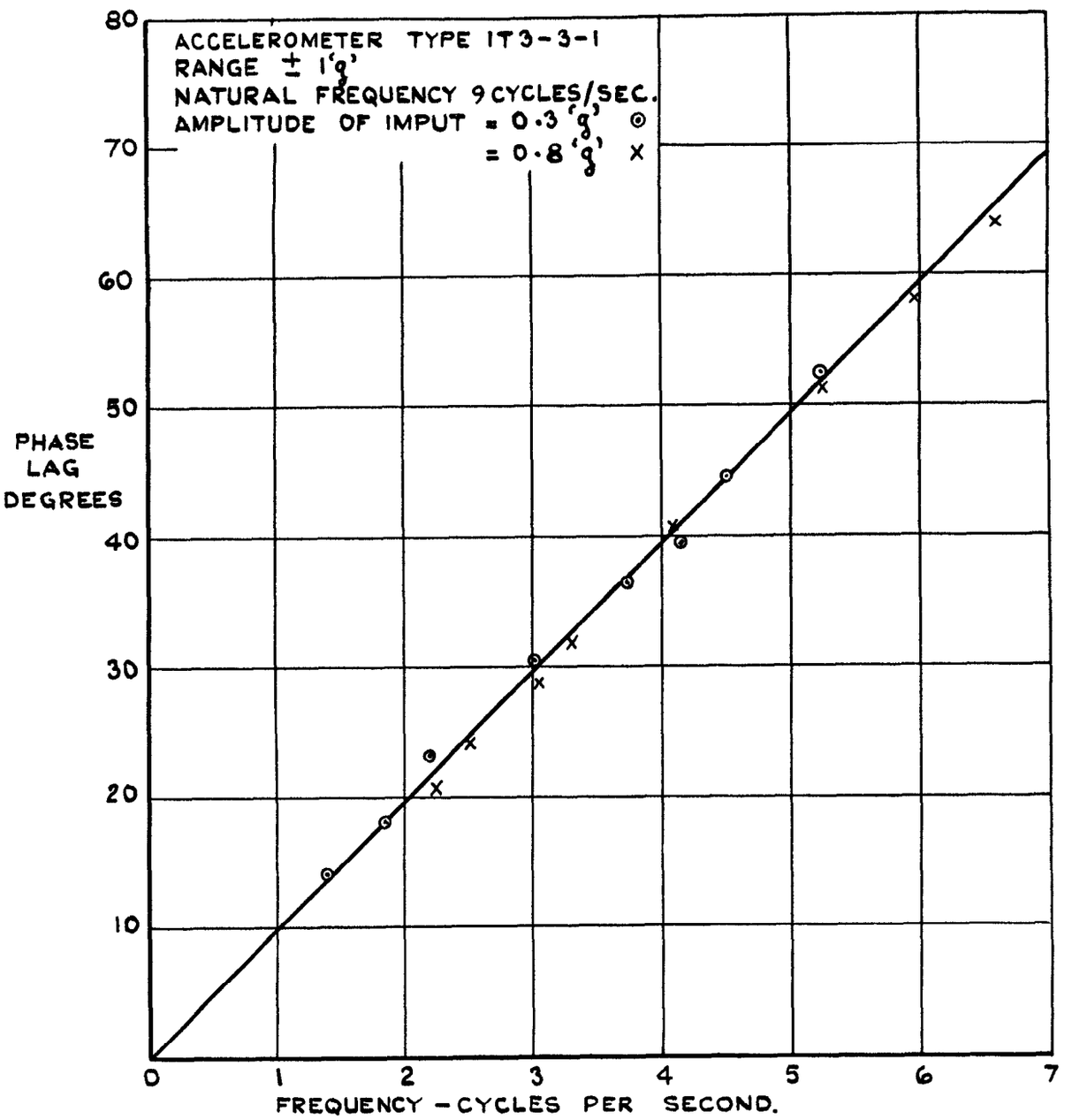

FIG. 3. PHASE LAG OF THE LATERAL ACCELEROMETER READING FROM A DYNAMIC CALIBRATION.

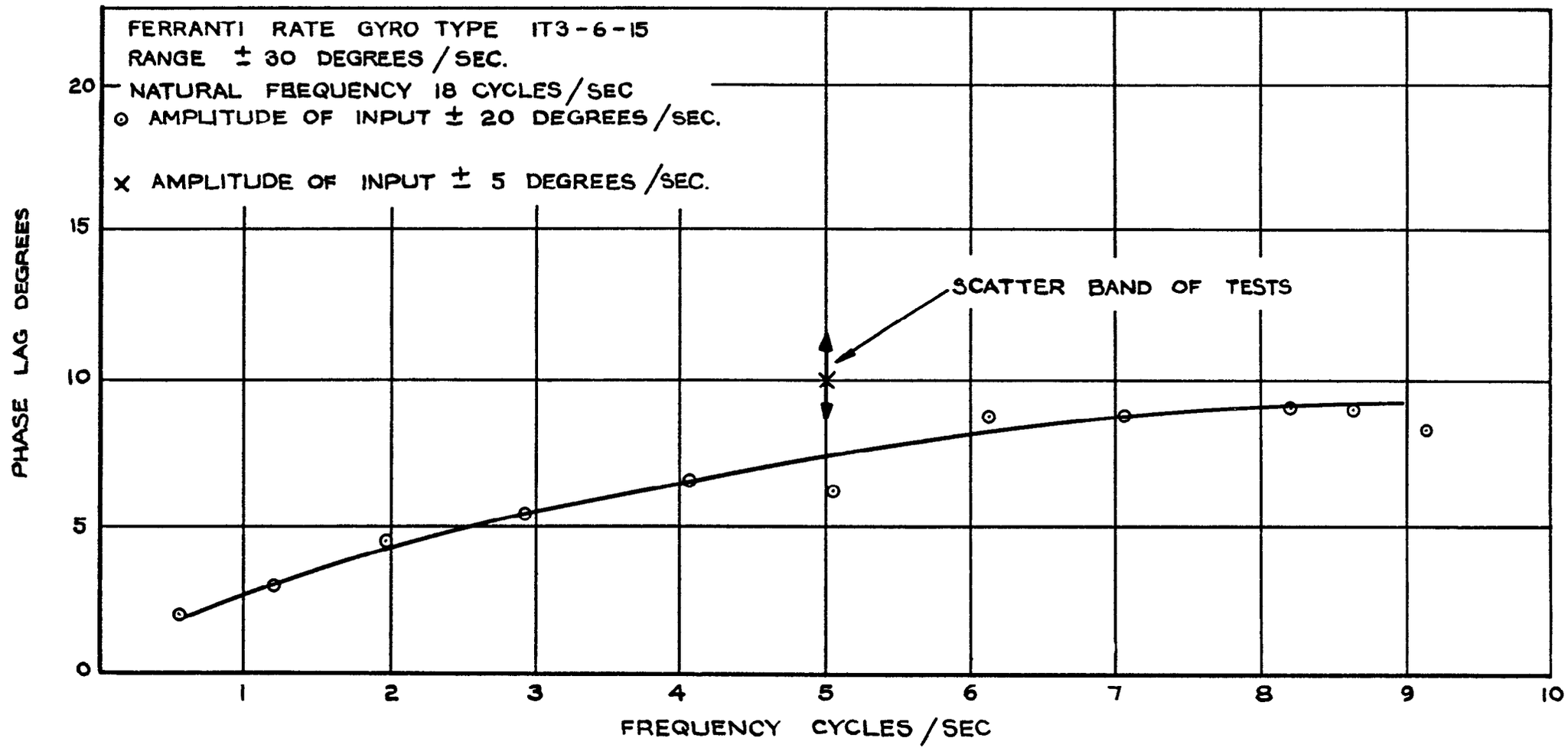

FIG. 4. PHASE LAG OF THE RATE OF ROLL GYRO READING FROM A DYNAMIC CALIBRATION.

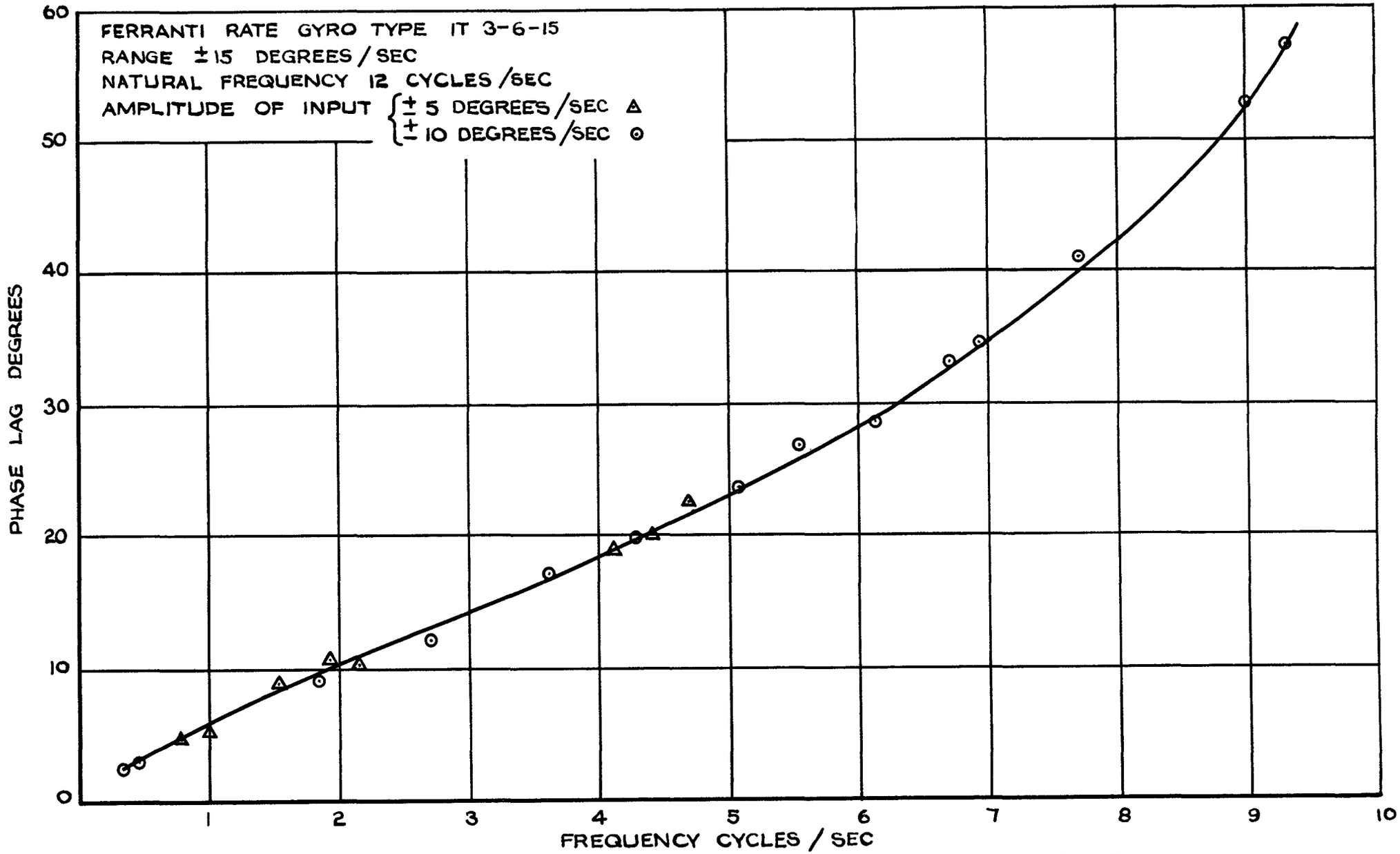

FIG. 5. PHASE LAG OF THE RATE OF YAW GYRO READING FROM A DYNAMIC CALIBRATION.

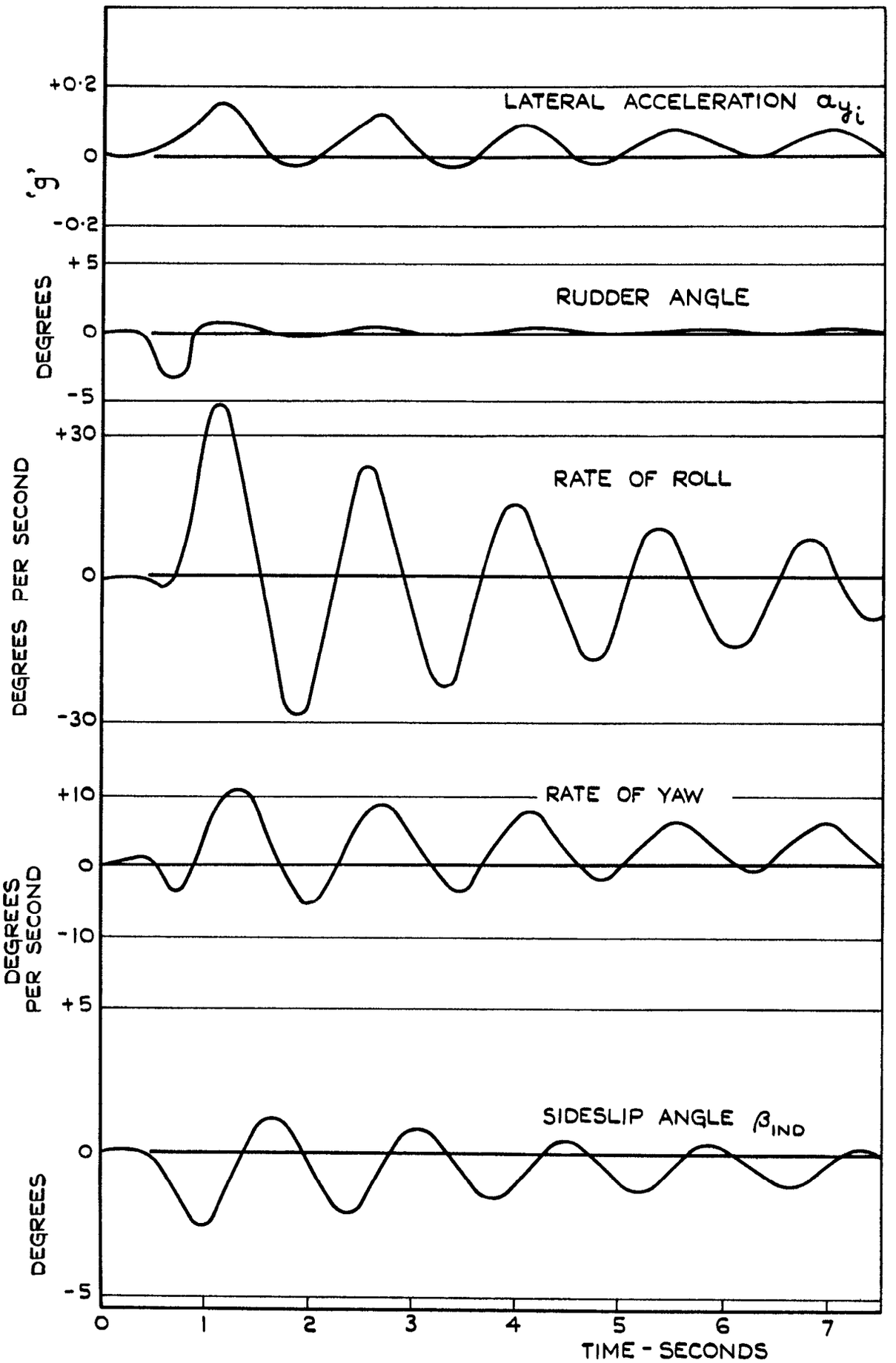

FIG. 6. TYPICAL FLIGHT RECORD OF THE VARIABLES DURING A DUTCH ROLL OSCILLATION.

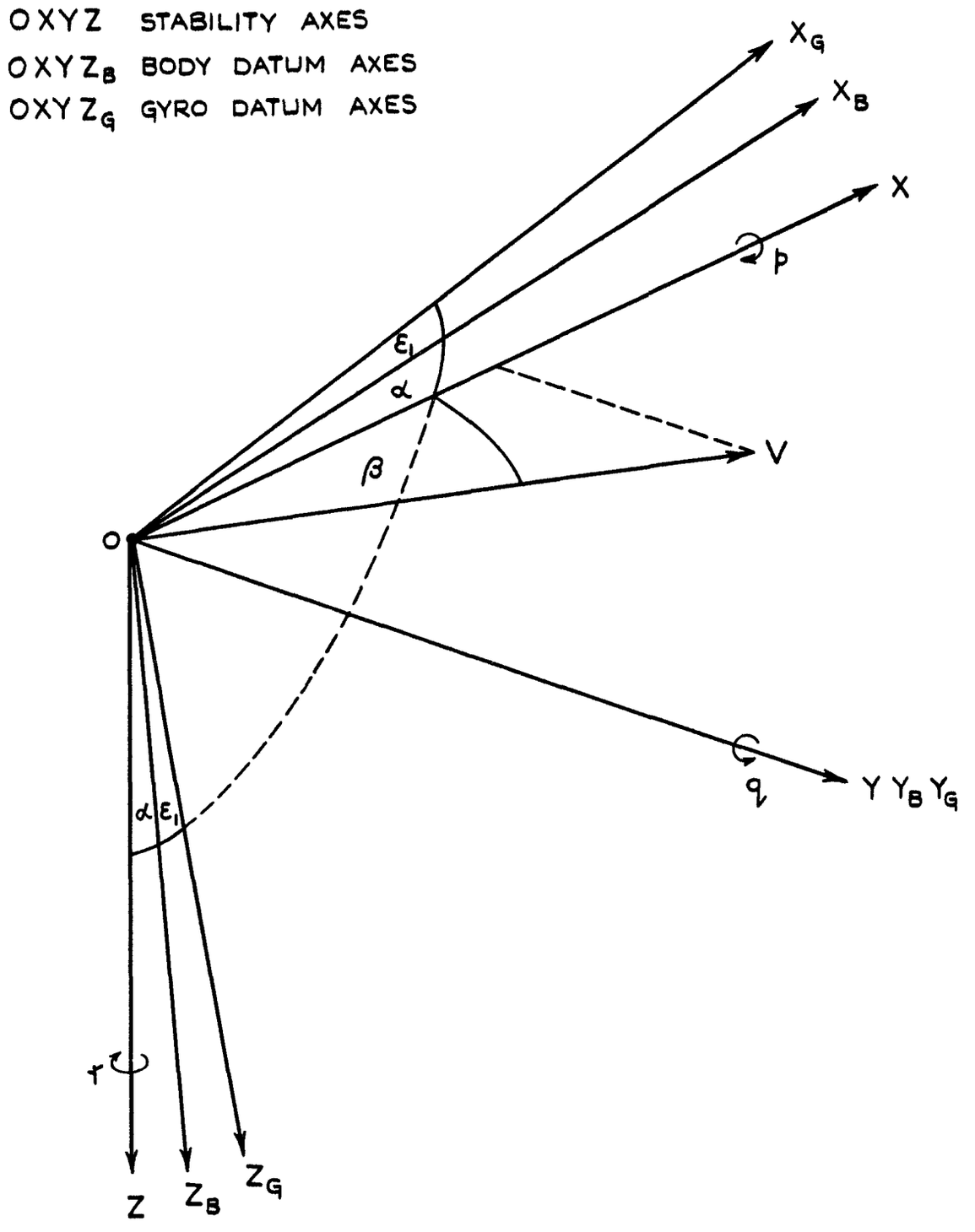

FIG. 7. SYSTEM OF STABILITY AND BODY DATUM AXES.

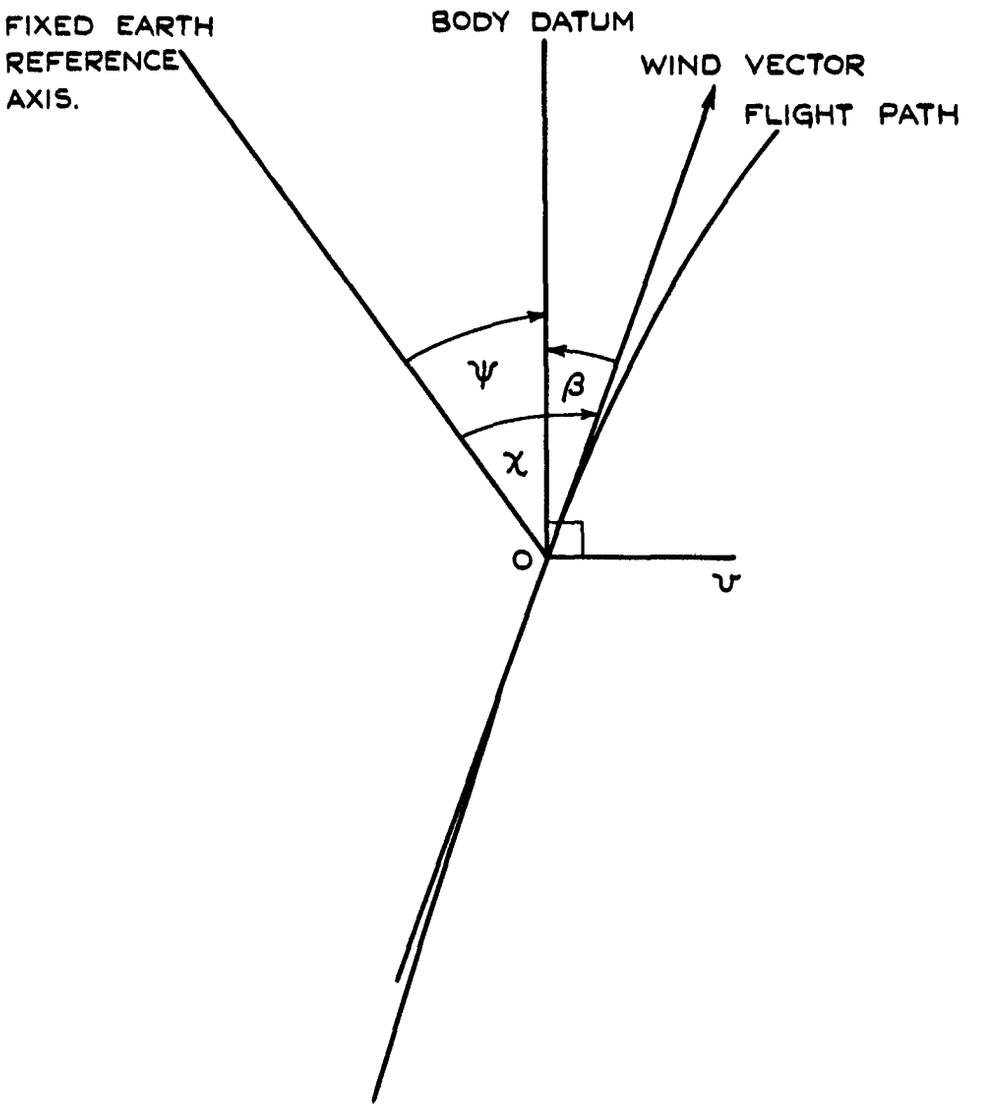

FIG. 8. DEFINITIONS OF SIDESLIP ANGLE, YAW ANGLE AND FLIGHT PATH ANGLE.

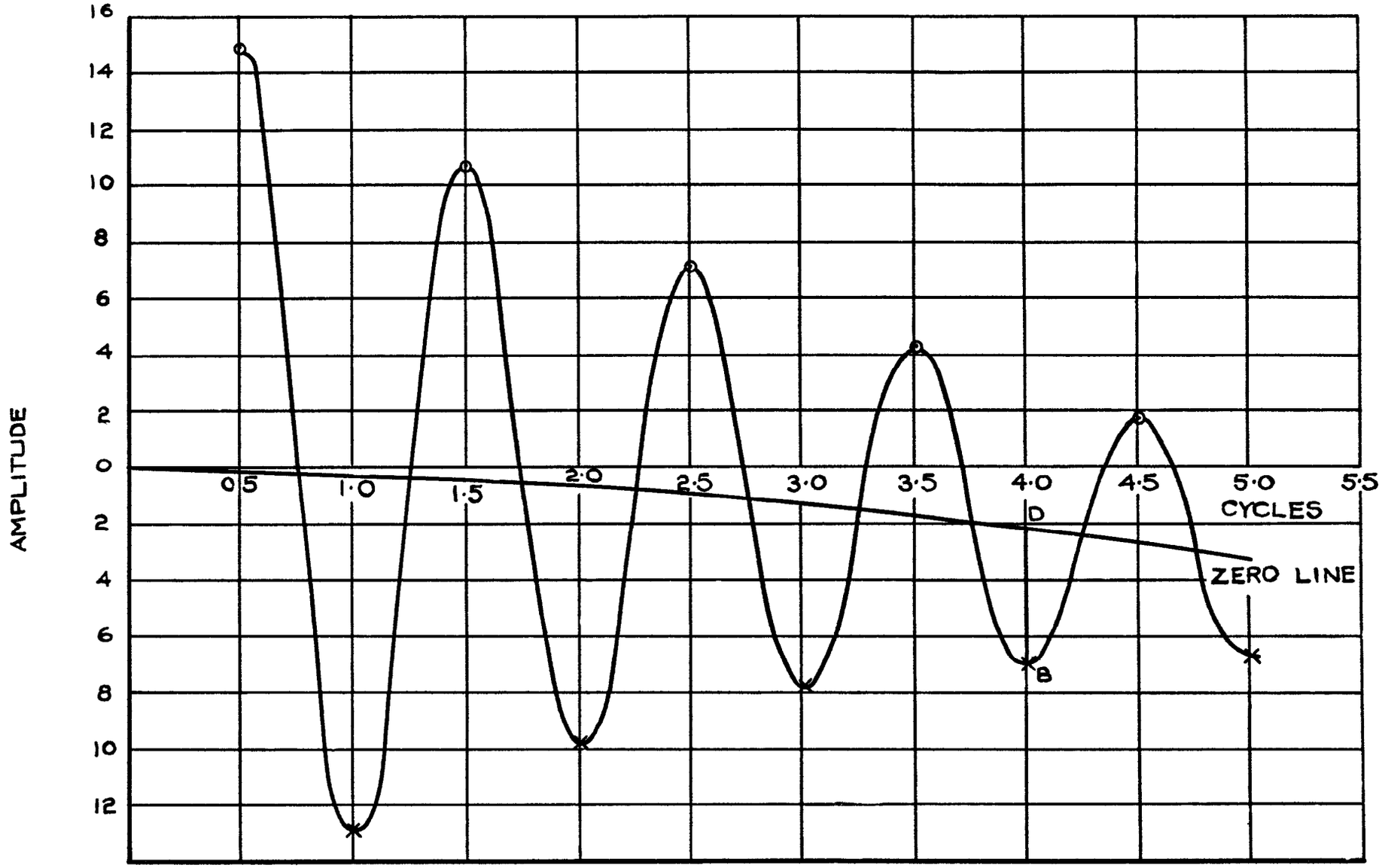

FIG. 9. TRUE ZERO LINE OF A DECAYING, SINUSOIDAL OSCILLATION SUPERIMPOSED ON A DIVERGENT MOTION (SPIRAL).

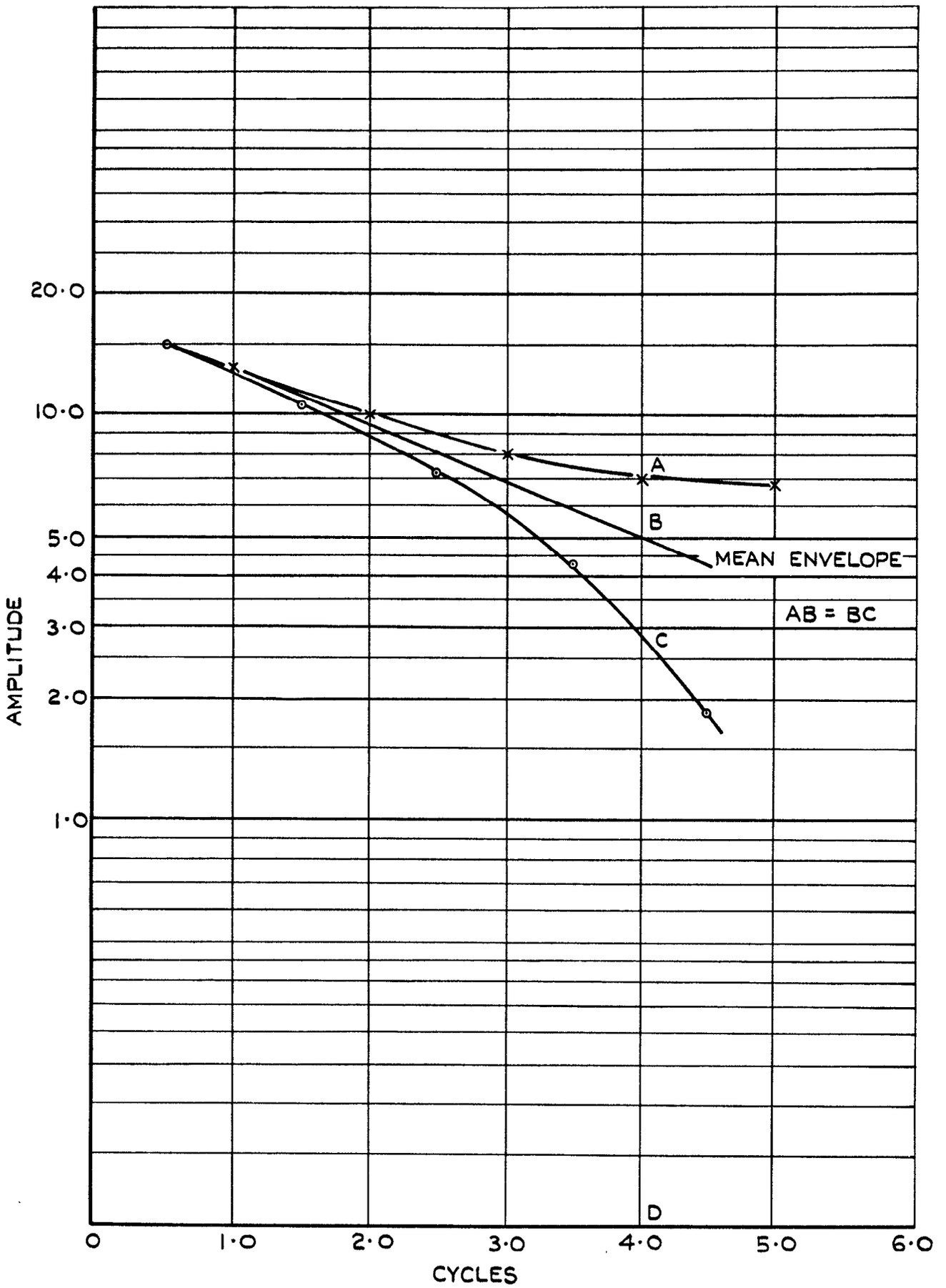

FIG. 10. LOGARITHMIC PLOT OF THE AMPLITUDES OF THE OSCILLATION REPRESENTED IN FIGURE 9.

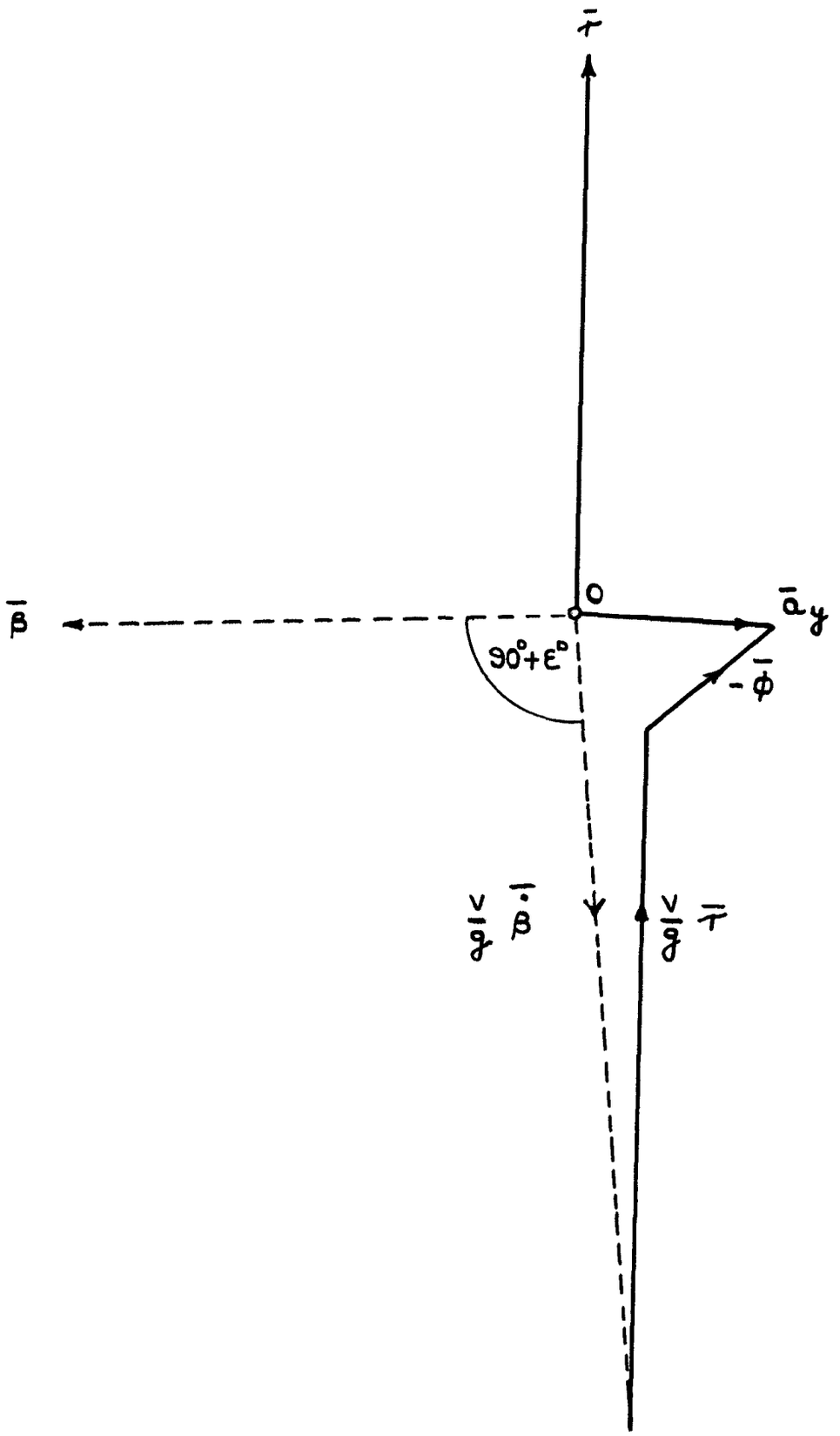

FIG. 11. DERIVATION OF SIDESLIP ANGLE BY A KINEMATIC RELATION.

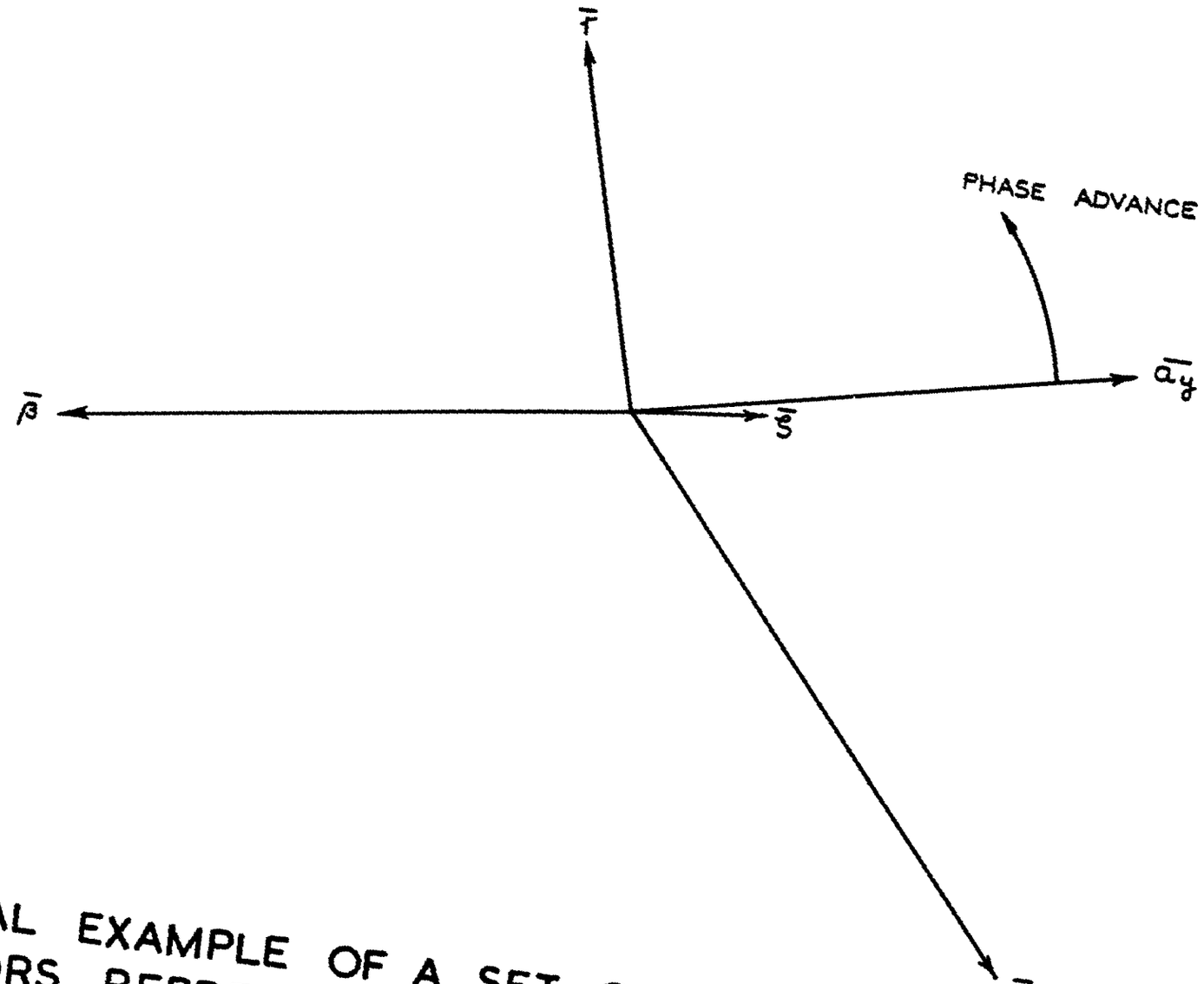

FIG. 12. TYPICAL EXAMPLE OF A SET OF FULLY CORRECTED TIME VECTORS REPRESENTING THE VARIABLES IN THE DUTCH ROLL OSCILLATION.

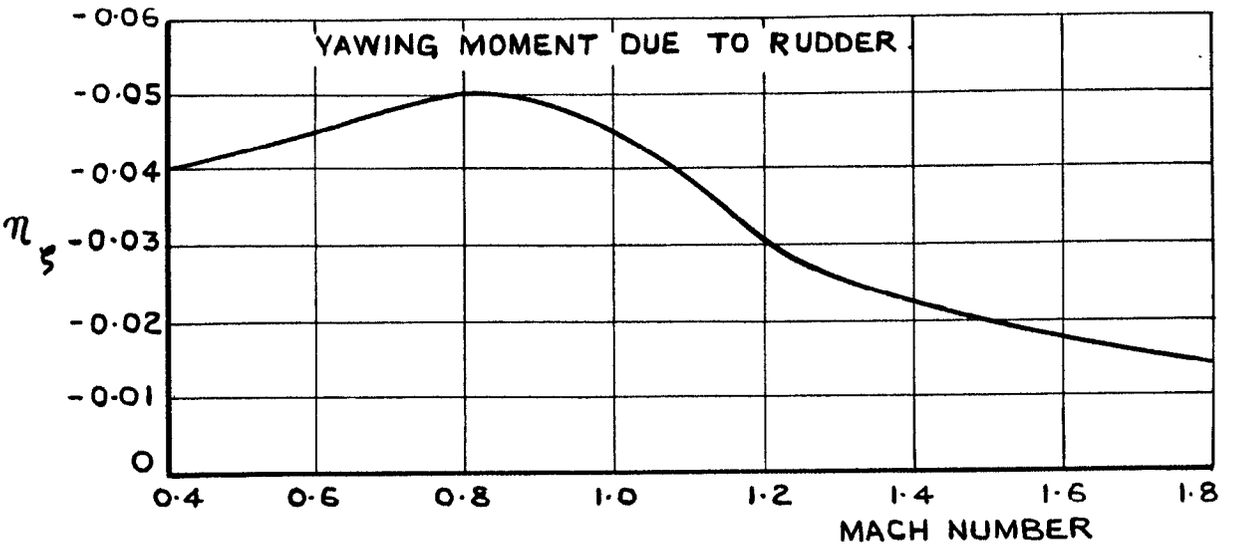

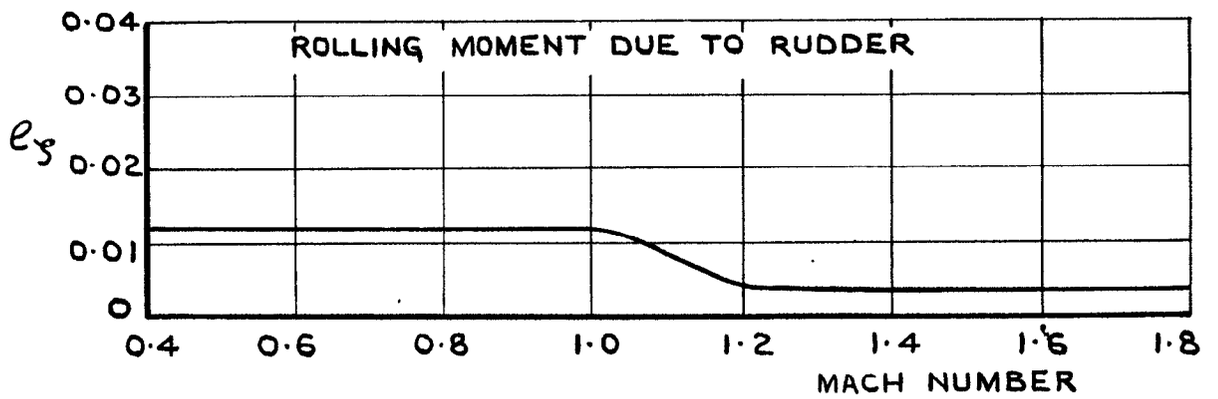

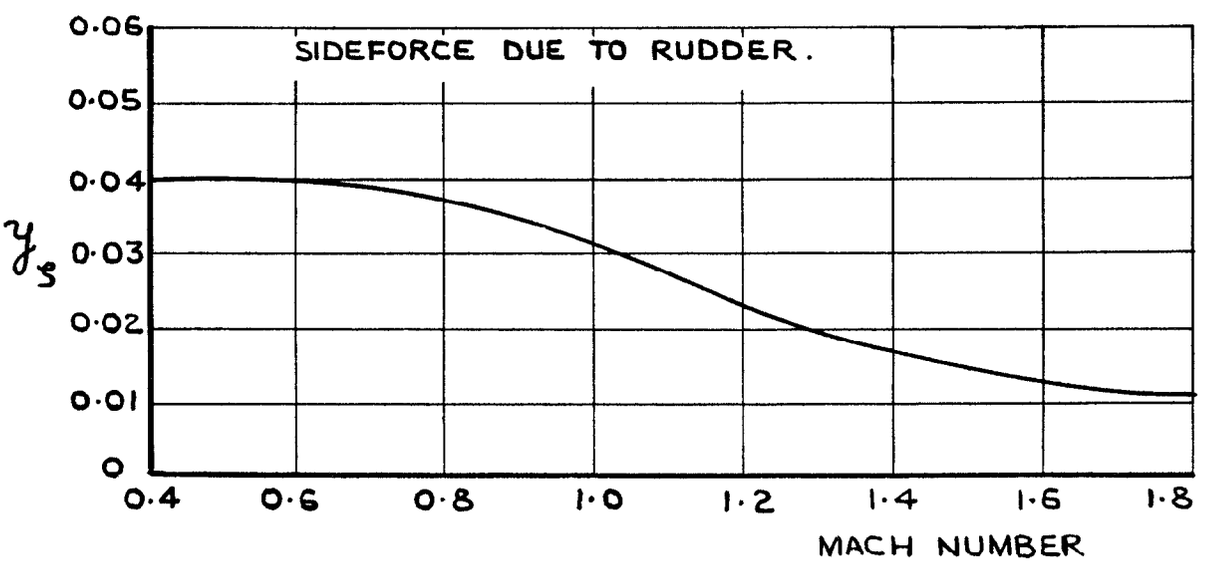

FIG. 13. ASSUMED VARIATION OF RUDDER DERIVATIVES WITH MACH NUMBER.

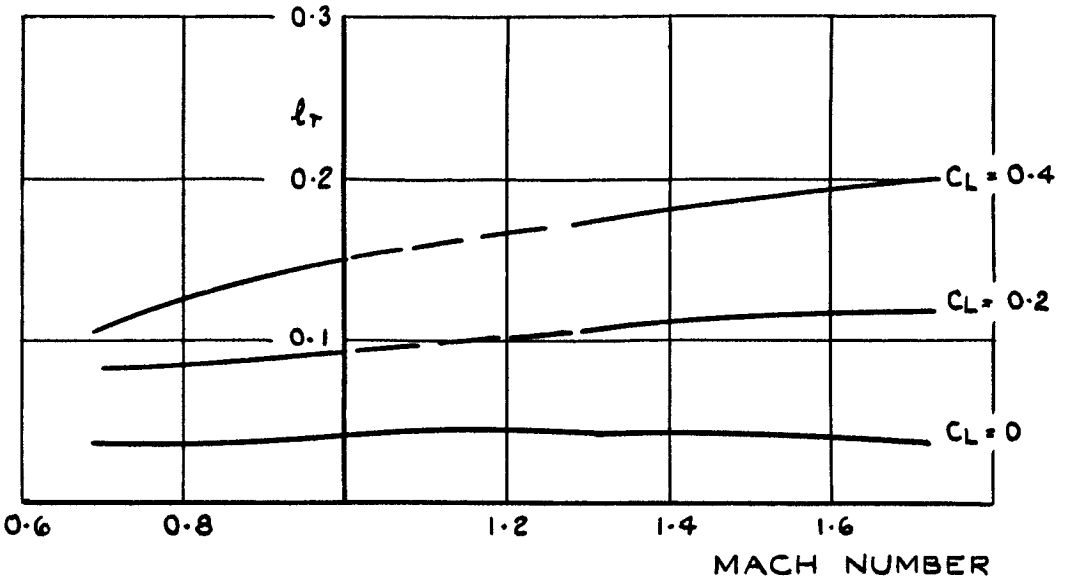

ROLLING MOMENT DUE TO YAWING l_r

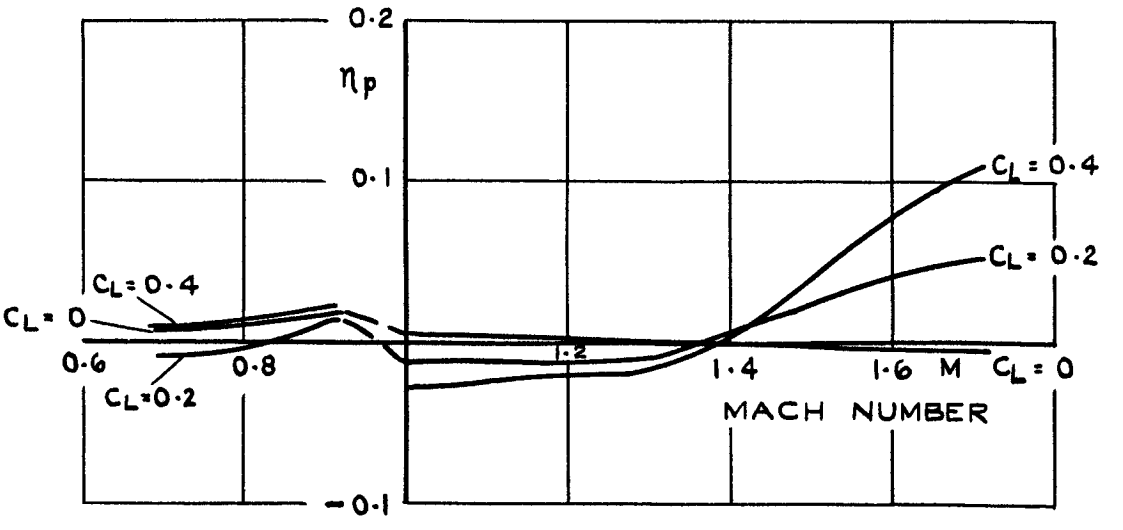

YAWING MOMENT DUE TO ROLLING n_p

KEY: ——— THEORY. — — — INTERPOLATION

FIG. 14. THEORETICAL ESTIMATE OF THE CROSS DERIVATIVES l_r AND n_p

ROLLING MOMENT EQUATION

$$L_\beta \cdot \bar{\beta} + L_p \cdot \bar{p} + L_r \cdot \bar{r} + L_\zeta \bar{\zeta} - A \dot{\bar{p}} + E \dot{\bar{r}} = 0$$

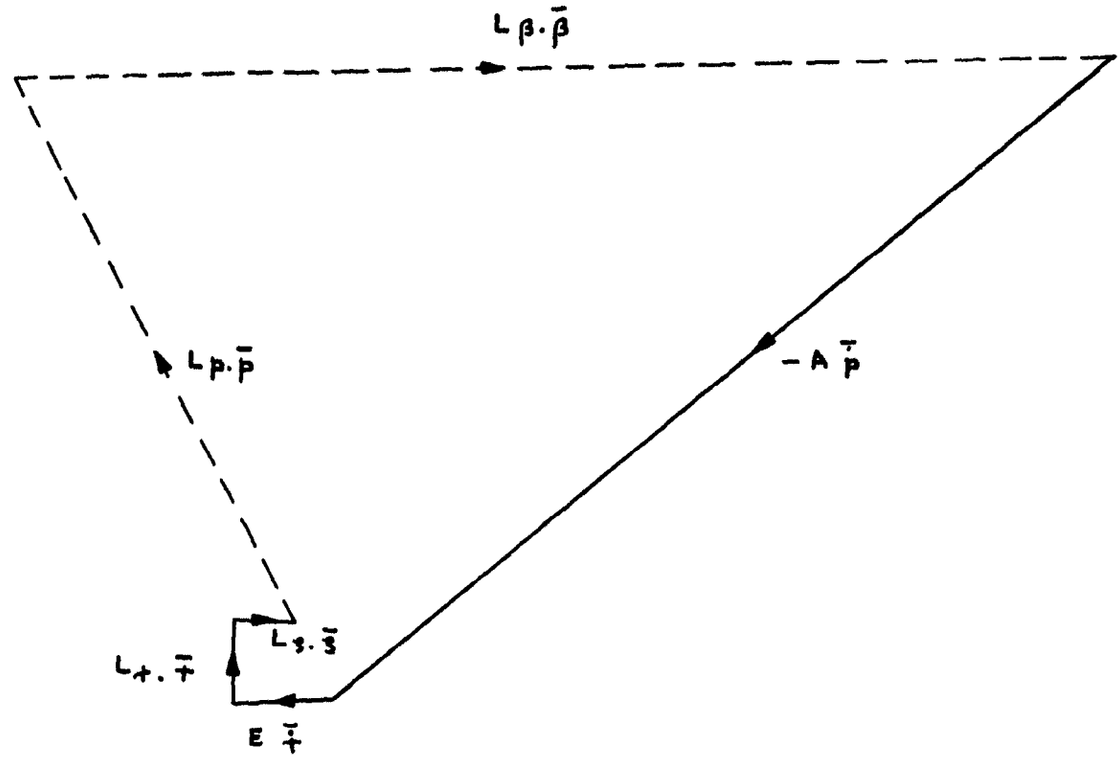

FIG. 15. ROLLING MOMENT VECTOR POLYGON.

YAWING MOMENT EQUATION

$$N_\beta . \bar{\beta} + N_r . \bar{r} + N_p . \bar{p} + N_\zeta . \bar{\zeta} - C \dot{\bar{r}} + E \dot{\bar{p}} = 0$$

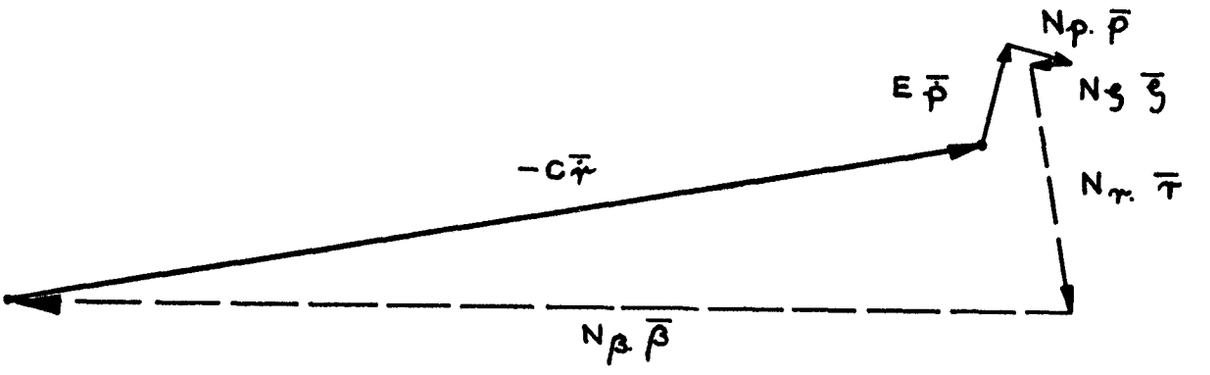

FIG. 16 YAWING MOMENT VECTOR POLYGON.

SIDEFORCE EQUATION

$$Y_\beta . \bar{\beta} + Y_\zeta . \bar{\zeta} - m . \bar{a}_y = 0$$

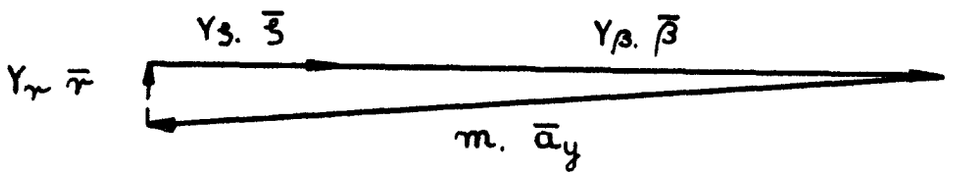

FIG. 17 SIDEFORCE VECTOR POLYGON.

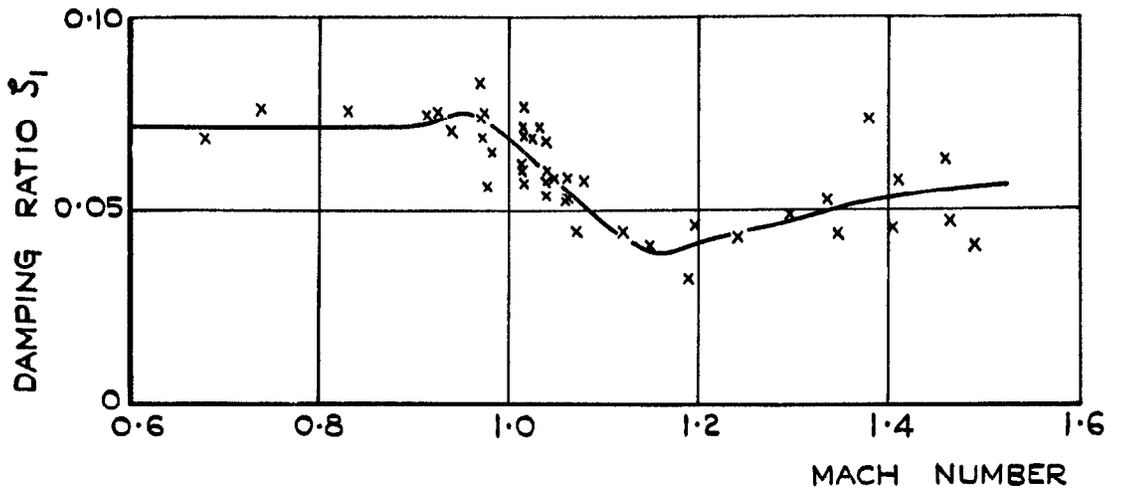

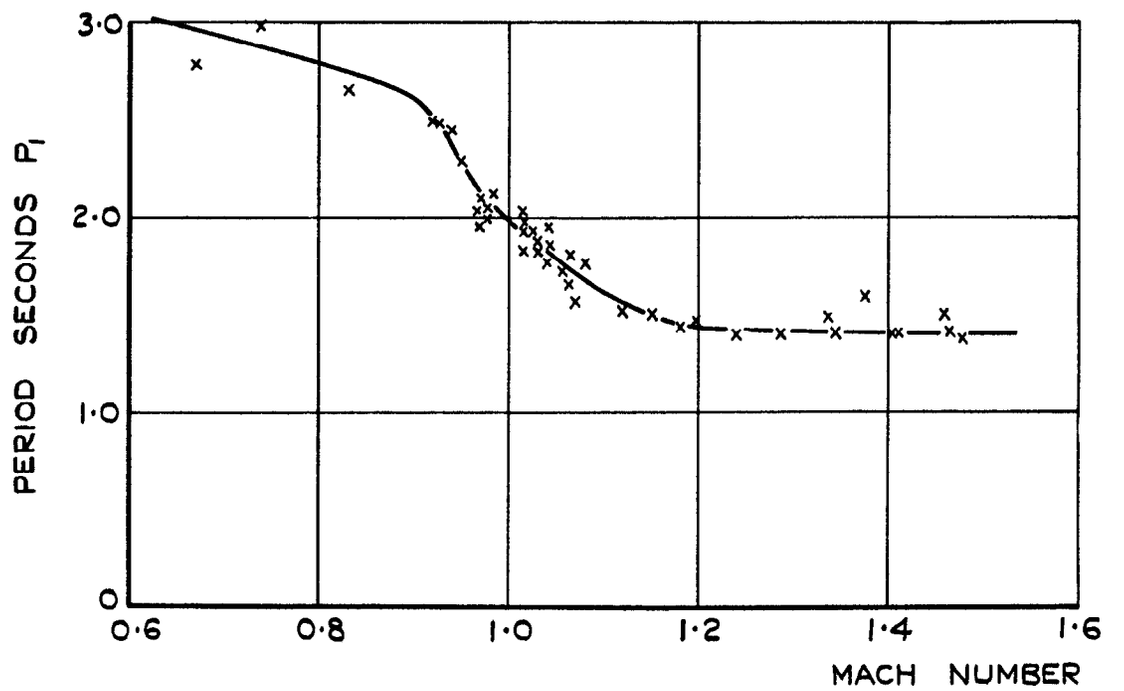

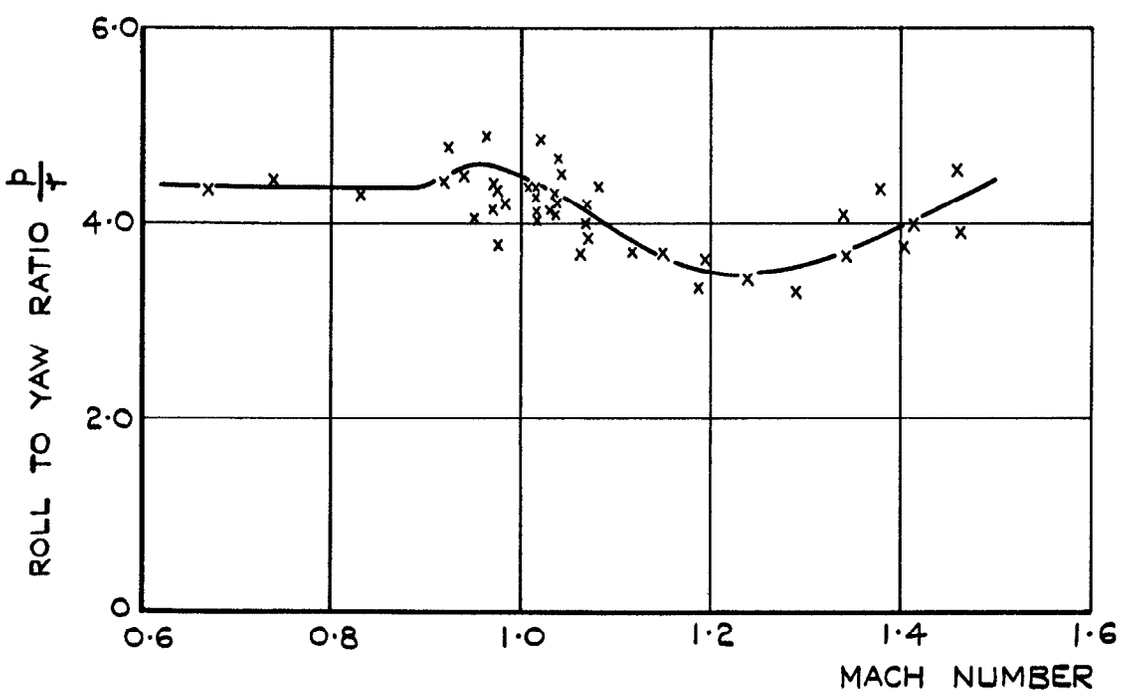

FIG. 18. CHARACTERISTICS OF THE DUTCH ROLL OSCILLATION IN LEVEL FLIGHT AT 40,000 FEET. FAIREY DELTA 2.

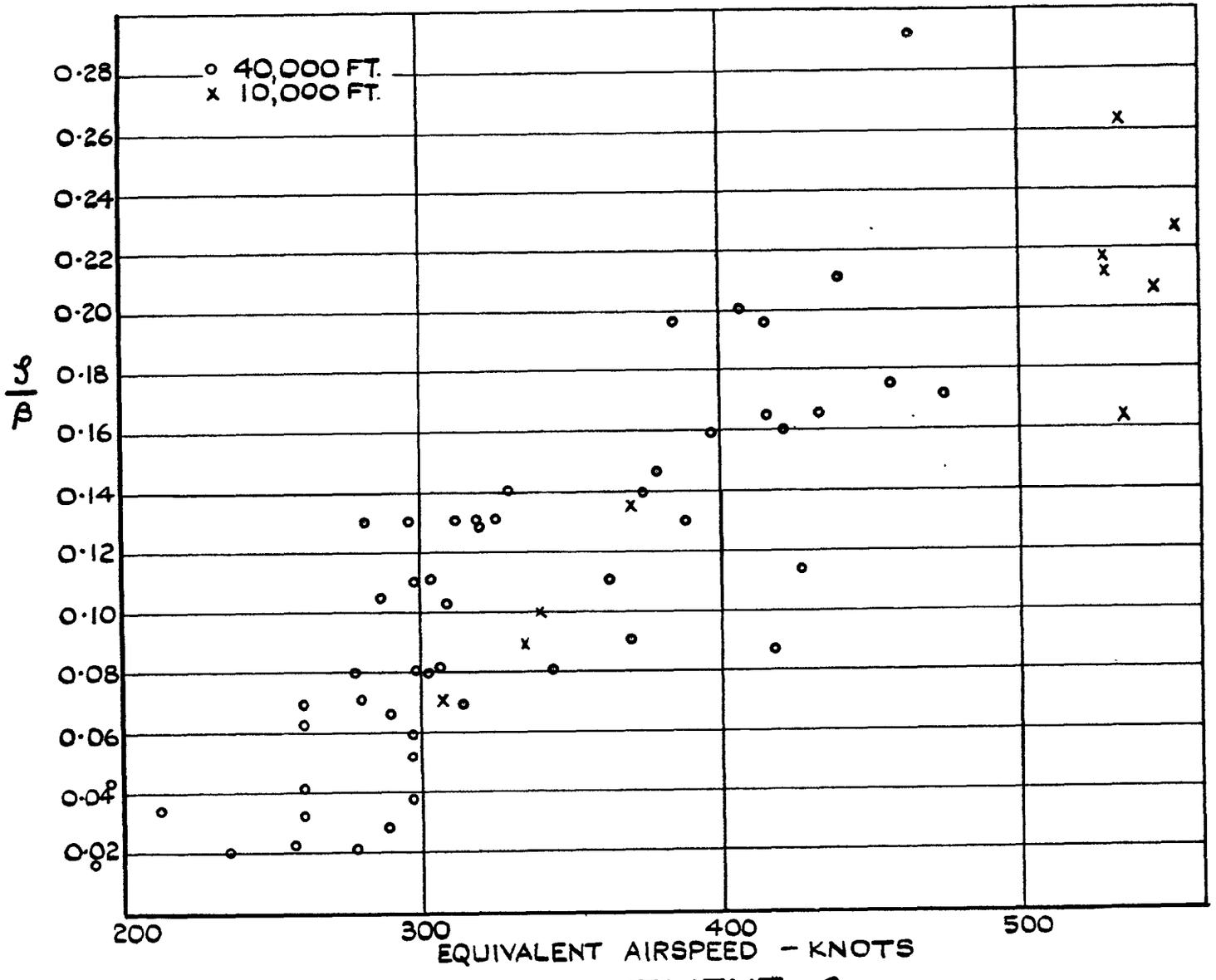

FIG.19. THE RATIO OF RUDDER MOVEMENT ζ TO SIDESLIP ANGLE β IN THE DUTCH ROLL OSCILLATION. FAIREY DELTA 2.

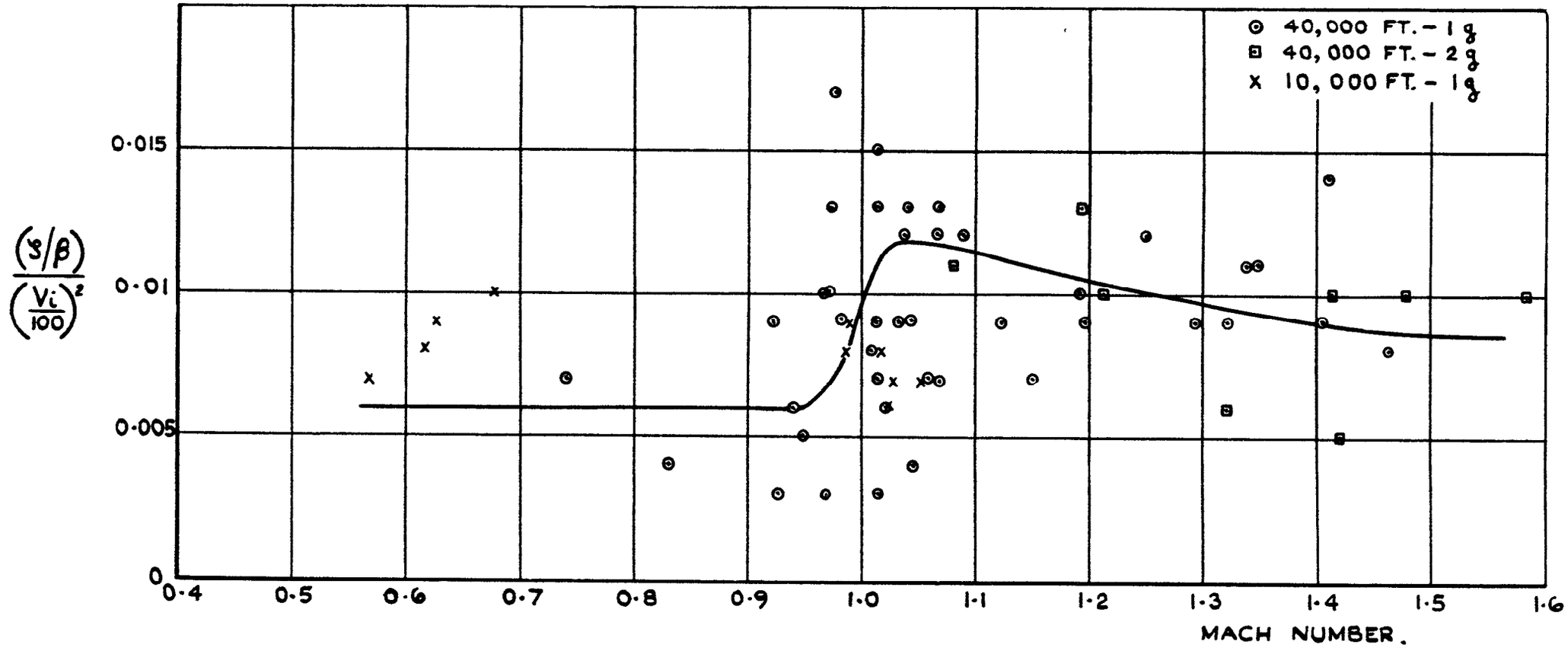

FIG. 20. THE VARIATION OF $\frac{(\zeta/\beta)}{\left(\frac{V_i}{100}\right)^2}$ WITH MACH NUMBER

FAIREY DELTA 2

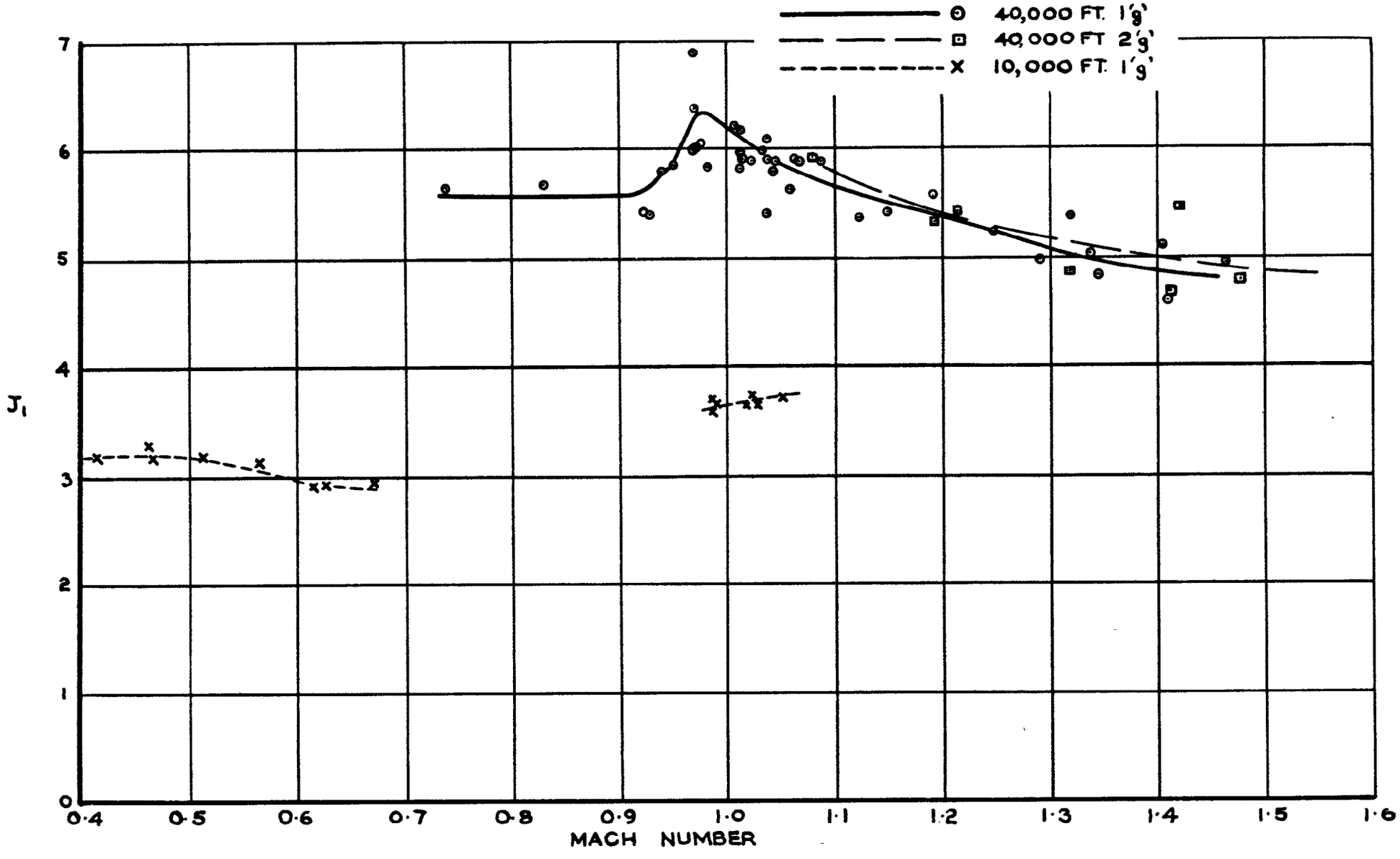

FIG. 21. THE NON-DIMENSIONAL FREQUENCY OF THE DUTCH ROLL OSCILLATION. FAIREY DELTA 2.

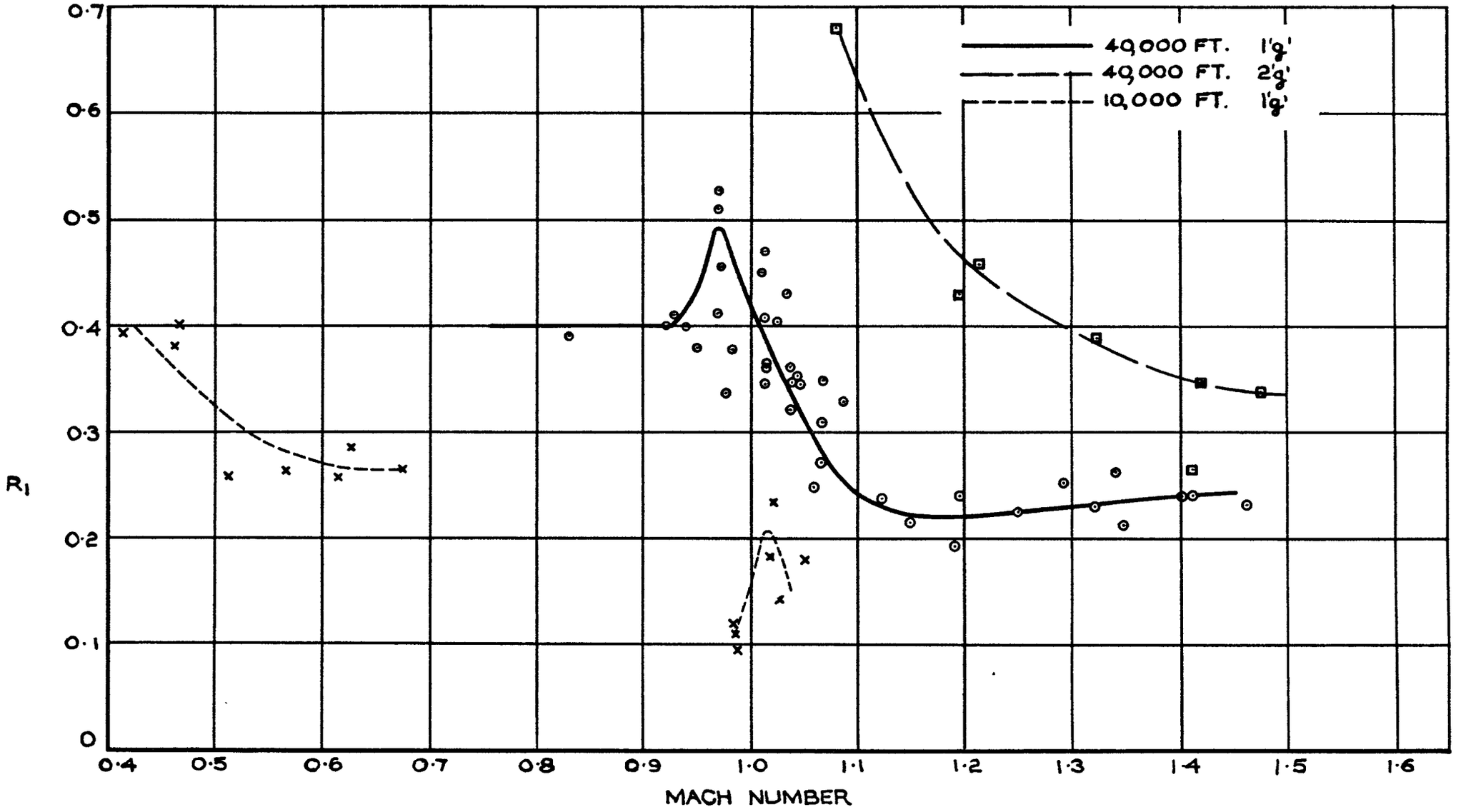

FIG. 22. THE NON DIMENSIONAL DAMPING FACTOR OF THE DUTCH ROLL OSCILLATION. FAIREY DELTA 2.

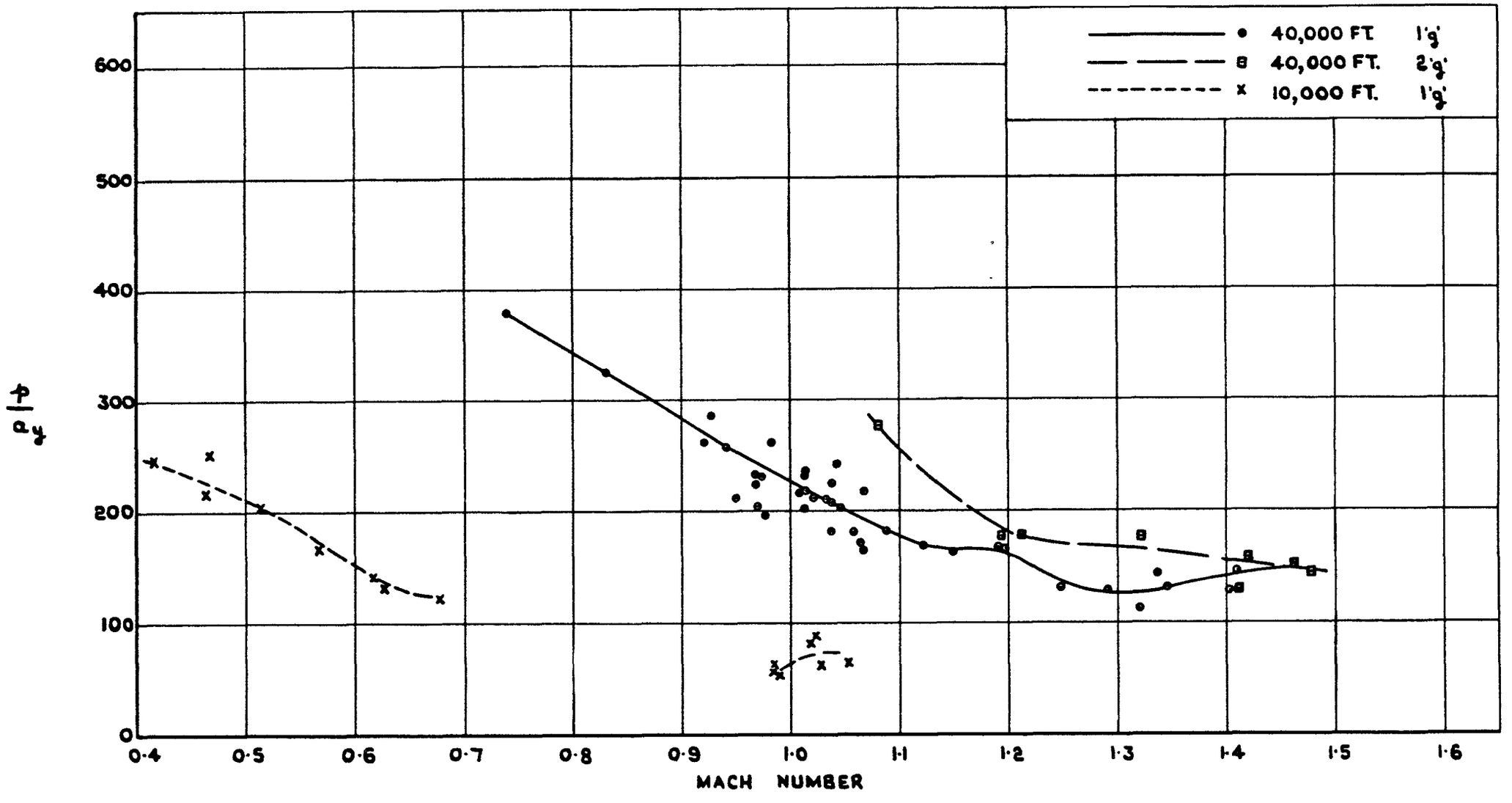

FIG. 23. THE RATIO OF RATE OF ROLL TO LATERAL ACCELERATION IN THE DUTCH ROLL OSCILLATION. FAIREY DELTA 2.

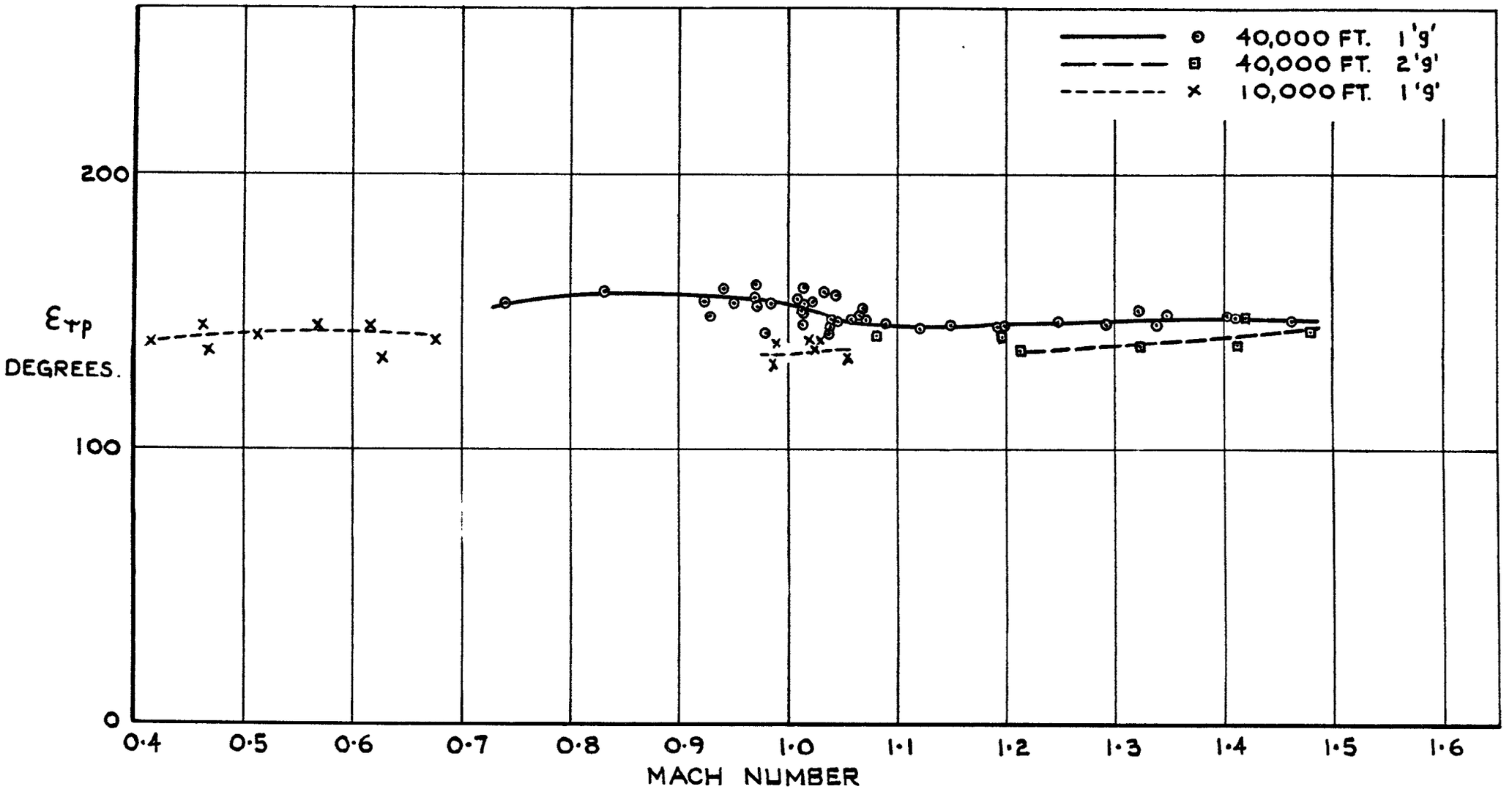

FIG. 24. THE PHASE LAG BETWEEN THE RATE OF YAW AND RATE OF ROLL IN THE DUTCH ROLL OSCILLATION. FAIREY DELTA 2.

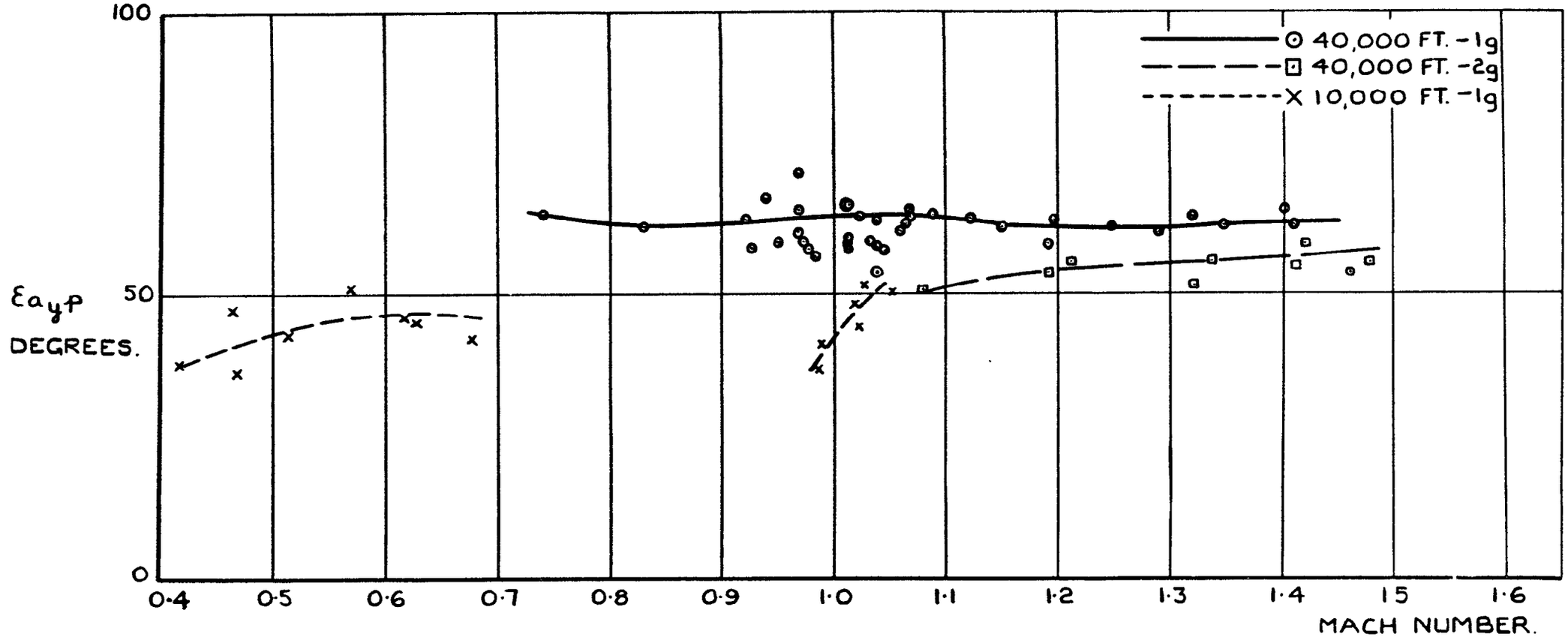

FIG. 25. THE PHASE LAG BETWEEN THE LATERAL ACCELERATION AND RATE OF ROLL IN THE DUTCH ROLL OSCILLATION FAIREY DELTA 2.

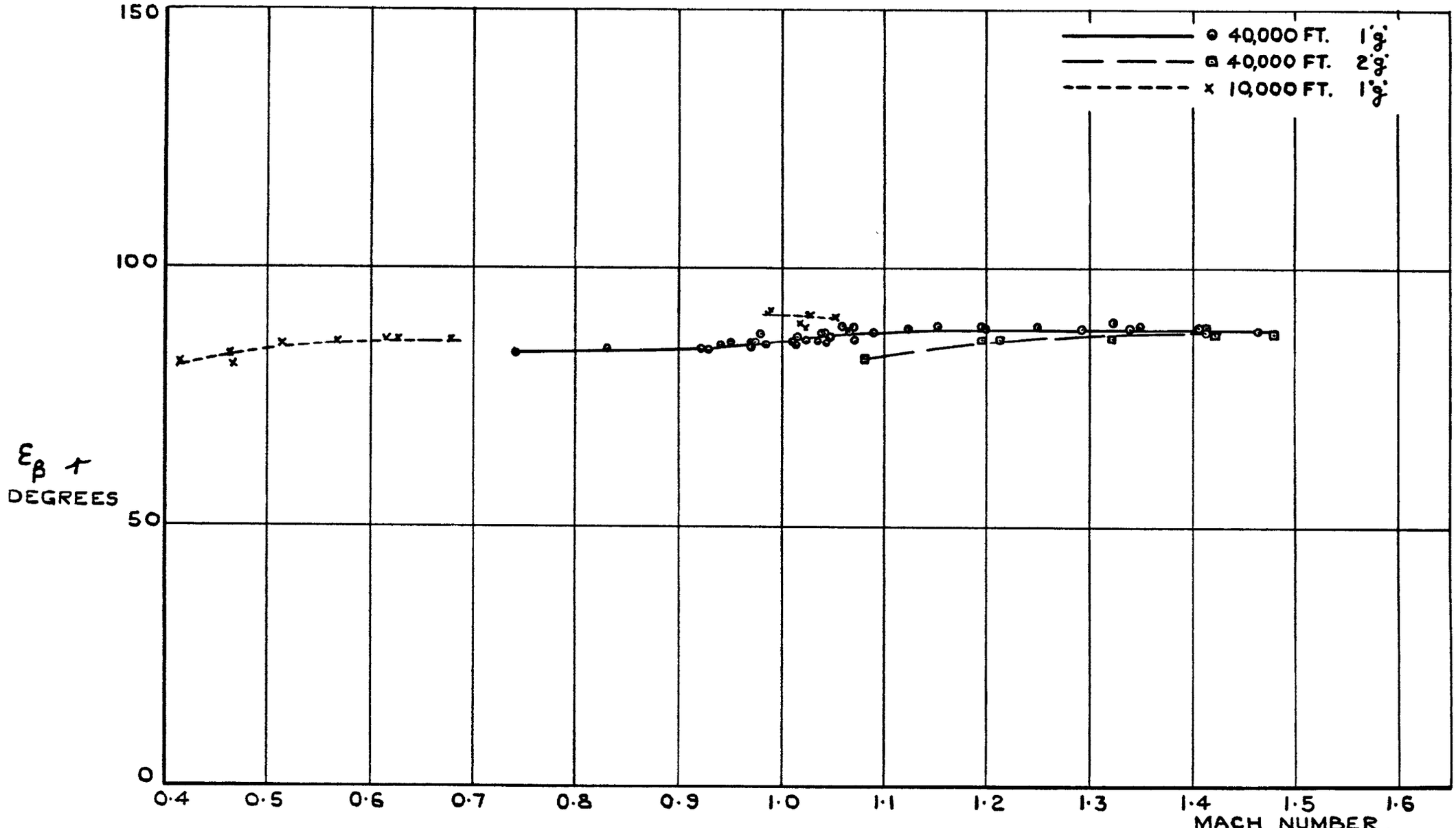

FIG. 26. THE PHASE LAG BETWEEN THE SIDESLIP ANGLE AND RATE OF YAW IN THE DUTCH ROLL OSCILLATION. FAIREY DELTA 2.

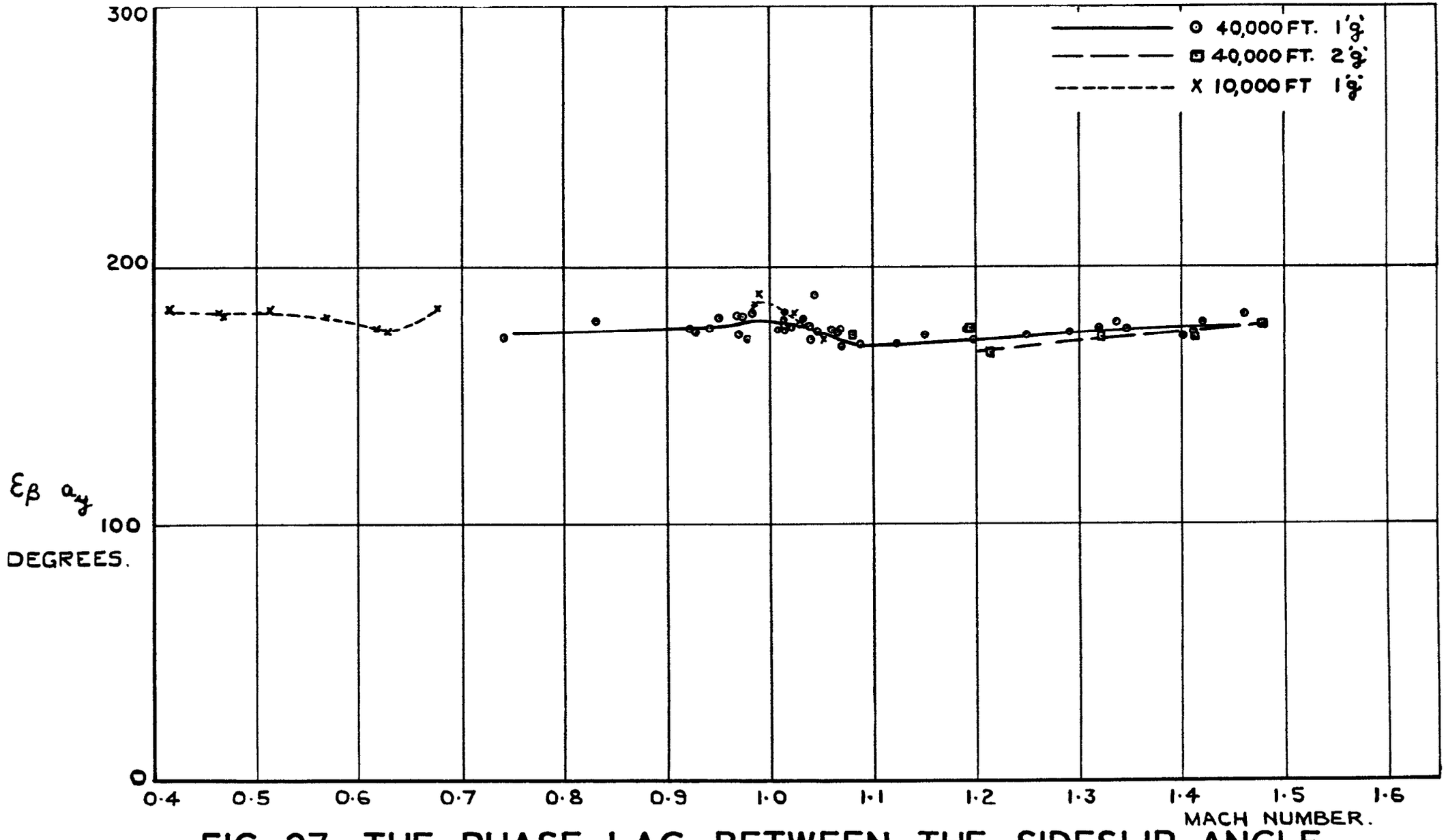

FIG. 27. THE PHASE LAG BETWEEN THE SIDESLIP ANGLE AND LATERAL ACCELERATION IN THE DUTCH ROLL OSCILLATION. FAIREY DELTA 2.

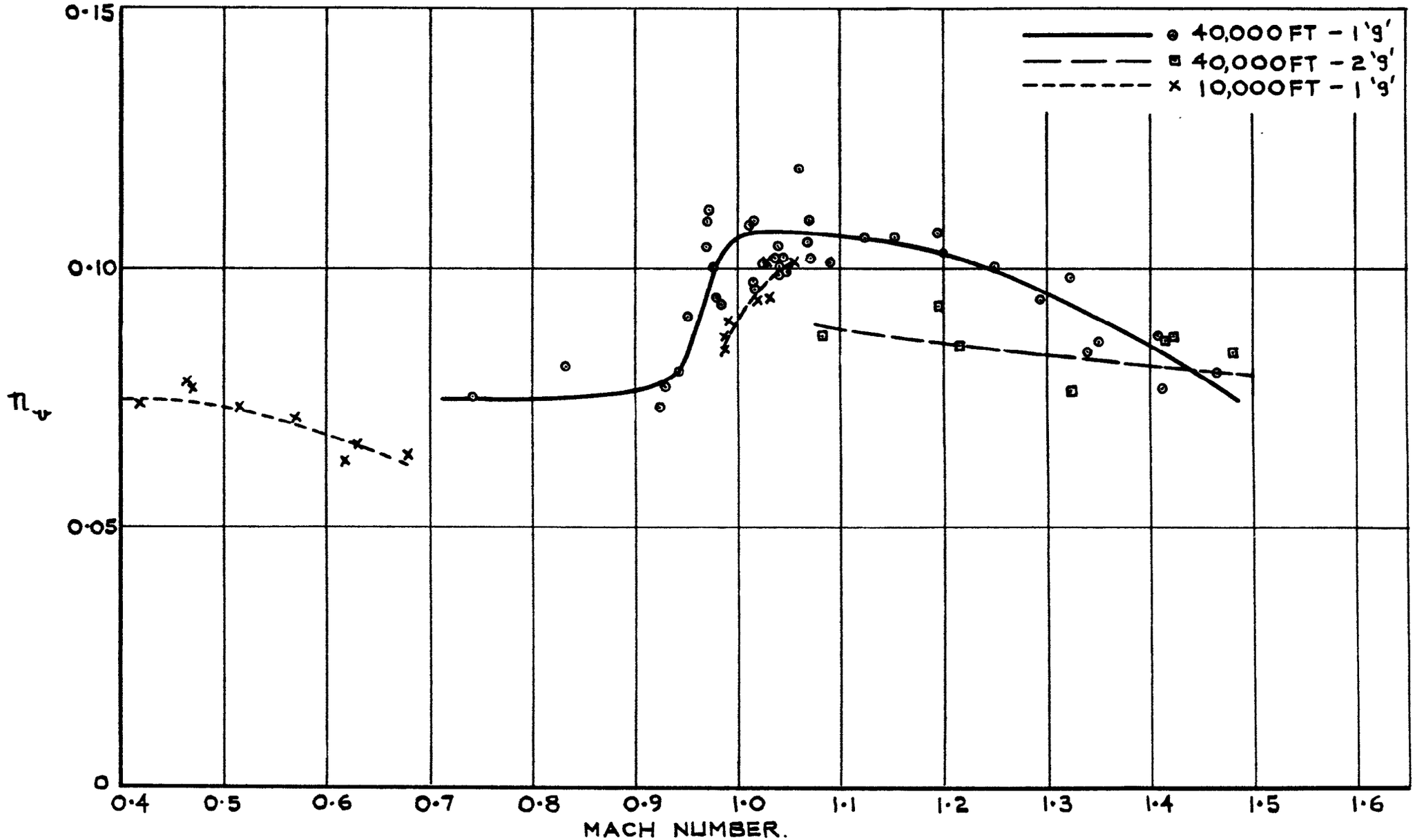

FIG. 28. VARIATION OF THE DIRECTIONAL STABILITY DERIVATIVE n_v WITH MACH NUMBER BY VECTOR ANALYSIS. FAIREY DELTA 2.

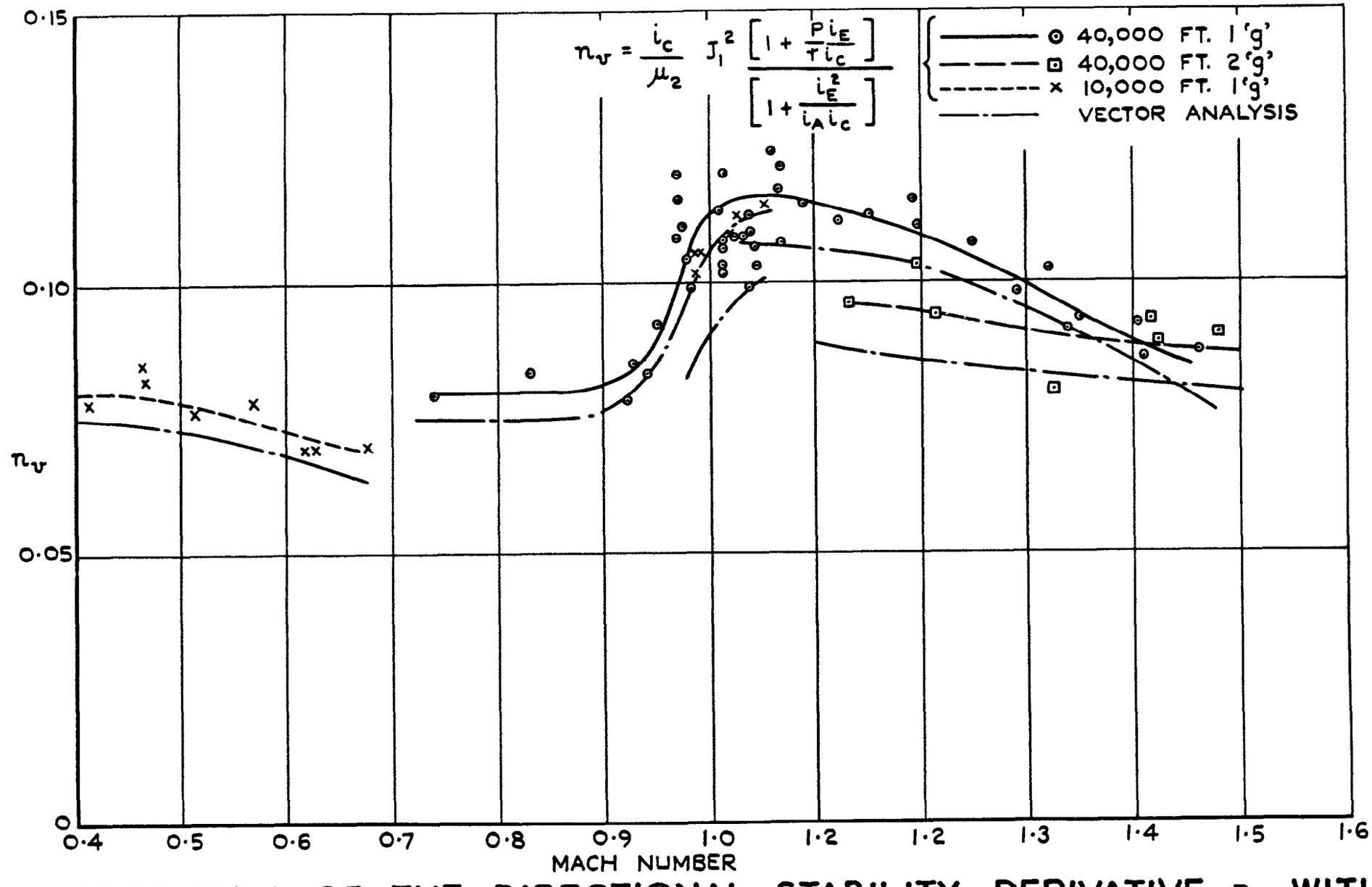

FIG. 29. VARIATION OF THE DIRECTIONAL STABILITY DERIVATIVE n_v WITH MACH NUMBER BY AN APPROXIMATION. FAIREY DELTA 2.

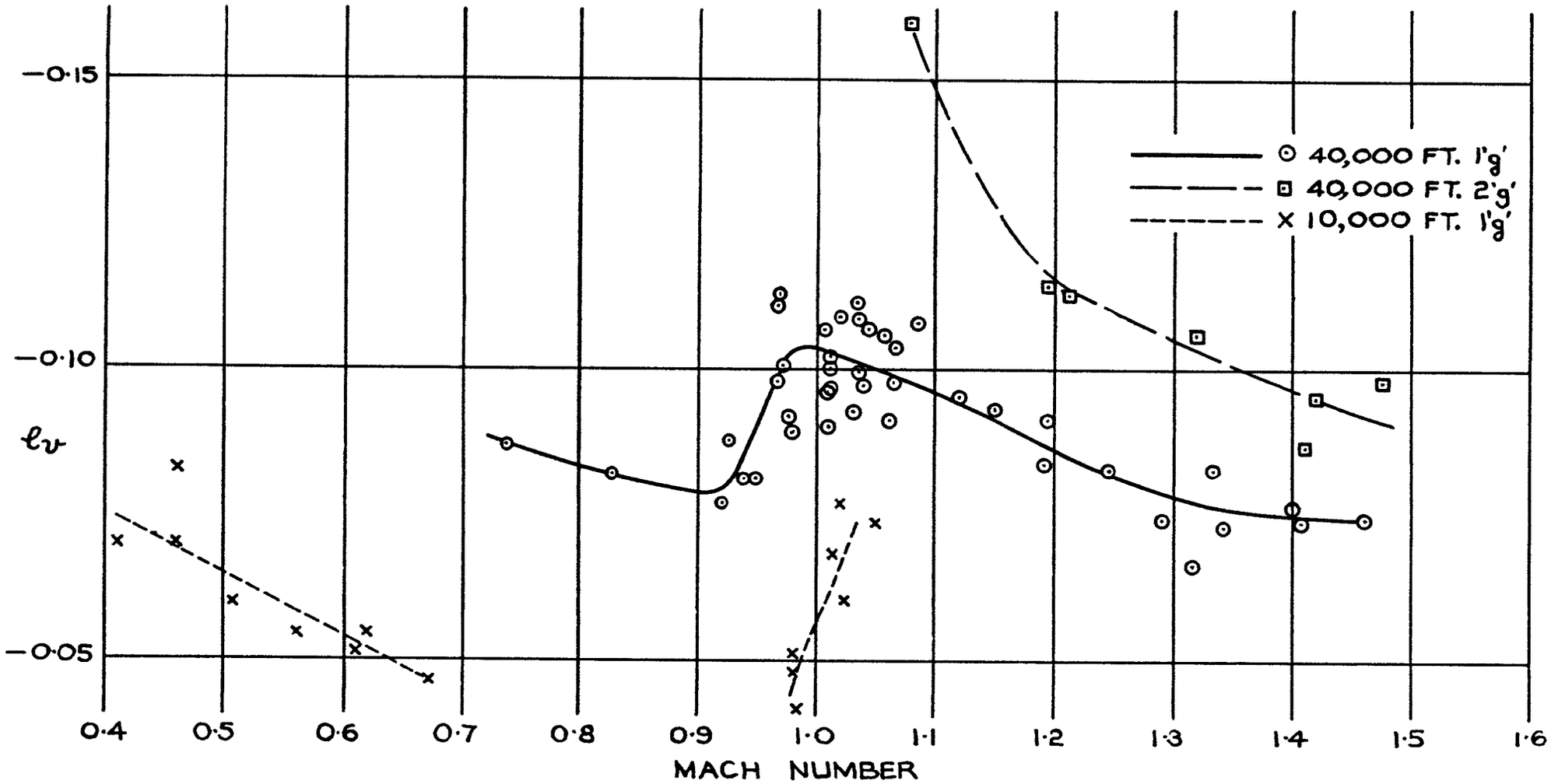

FIG. 30. VARIATION OF THE ROLLING MOMENT DUE TO SIDESLIP DERIVATIVE l_v WITH MACH NUMBER BY VECTOR ANALYSIS.
FAIREY DELTA 2.

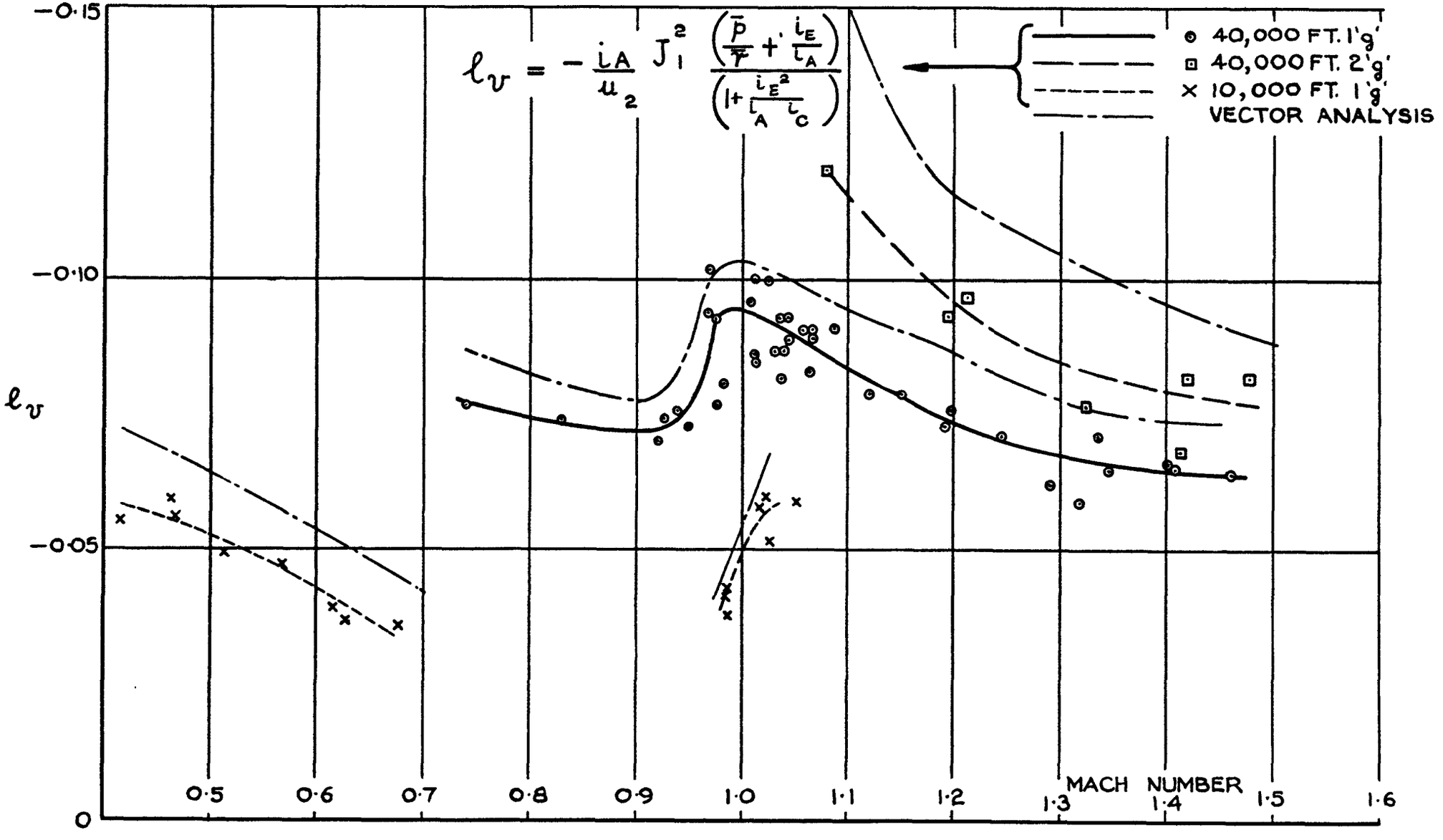

FIG. 31. VARIATION OF THE ROLLING MOMENT DUE TO SIDESLIP DERIVATIVE ℓ_v WITH MACH NUMBER BY AN APPROXIMATION. FAIREY DELTA 2.

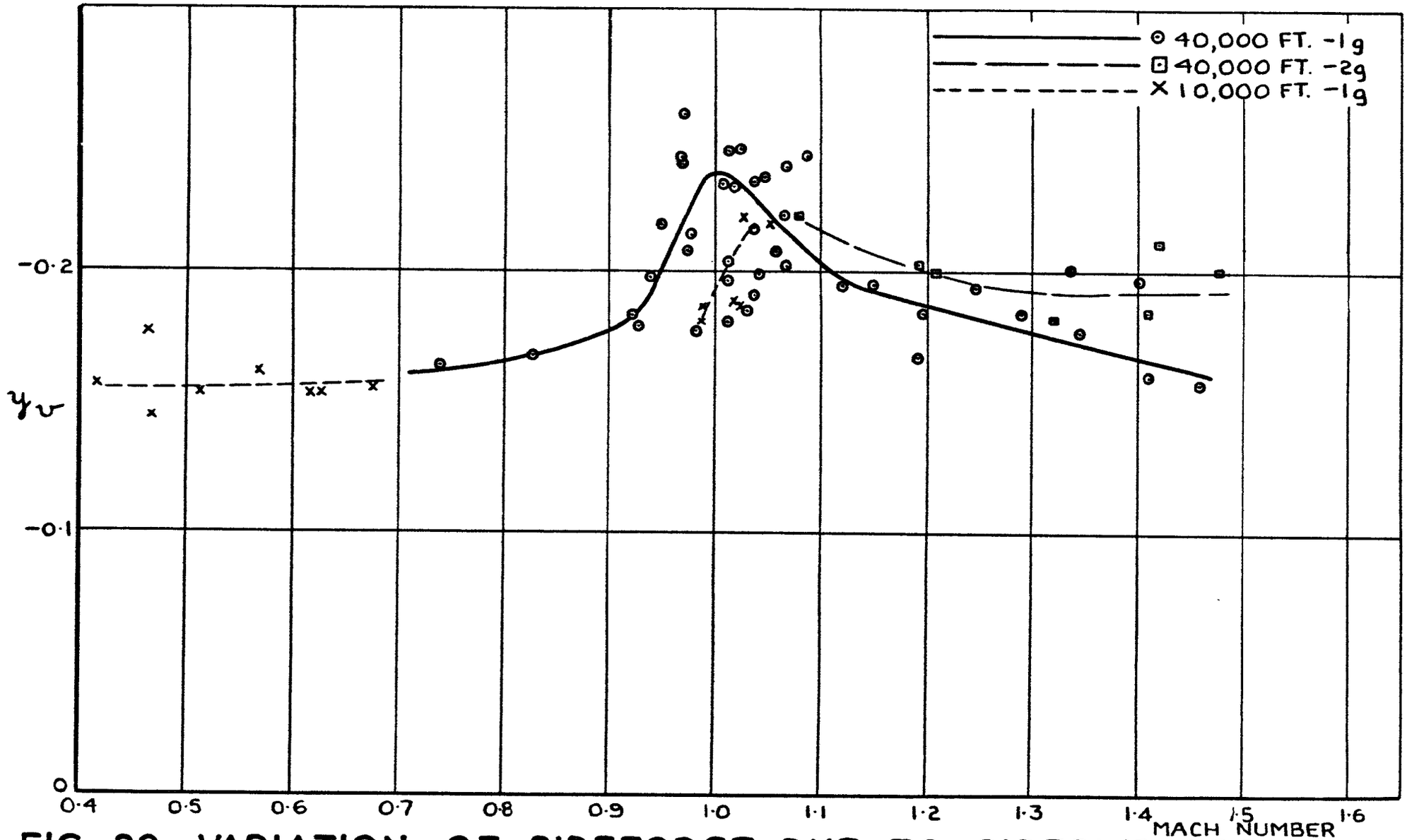

FIG. 32. VARIATION OF SIDEFORCE DUE TO SIDESLIP DERIVATIVE y_v WITH MACH NUMBER BY VECTOR ANALYSIS.
FAIREY DELTA 2.

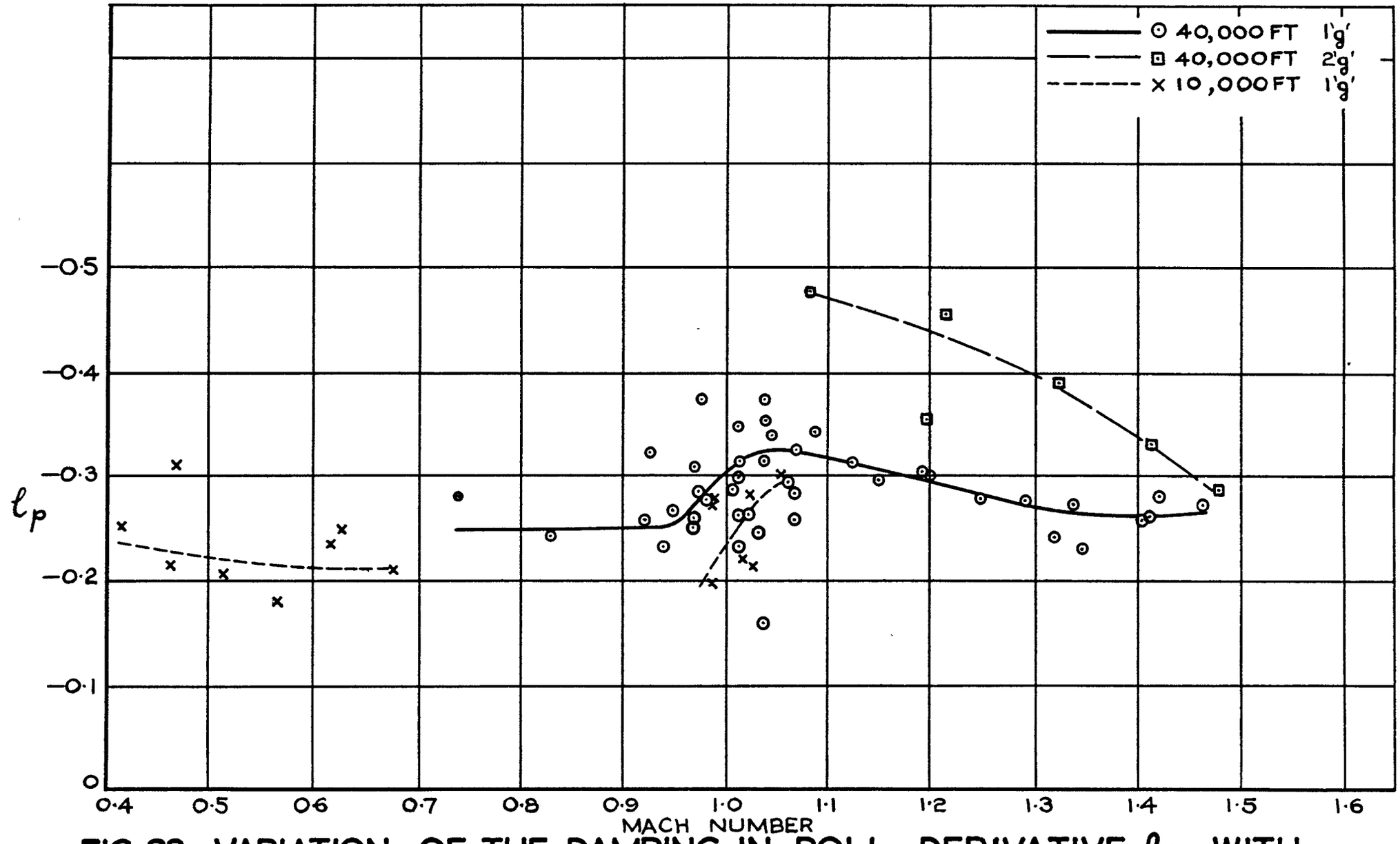

FIG. 33. VARIATION OF THE DAMPING IN ROLL DERIVATIVE l_p WITH MACH NUMBER BY VECTOR ANALYSIS.
FAIREY DELTA 2.

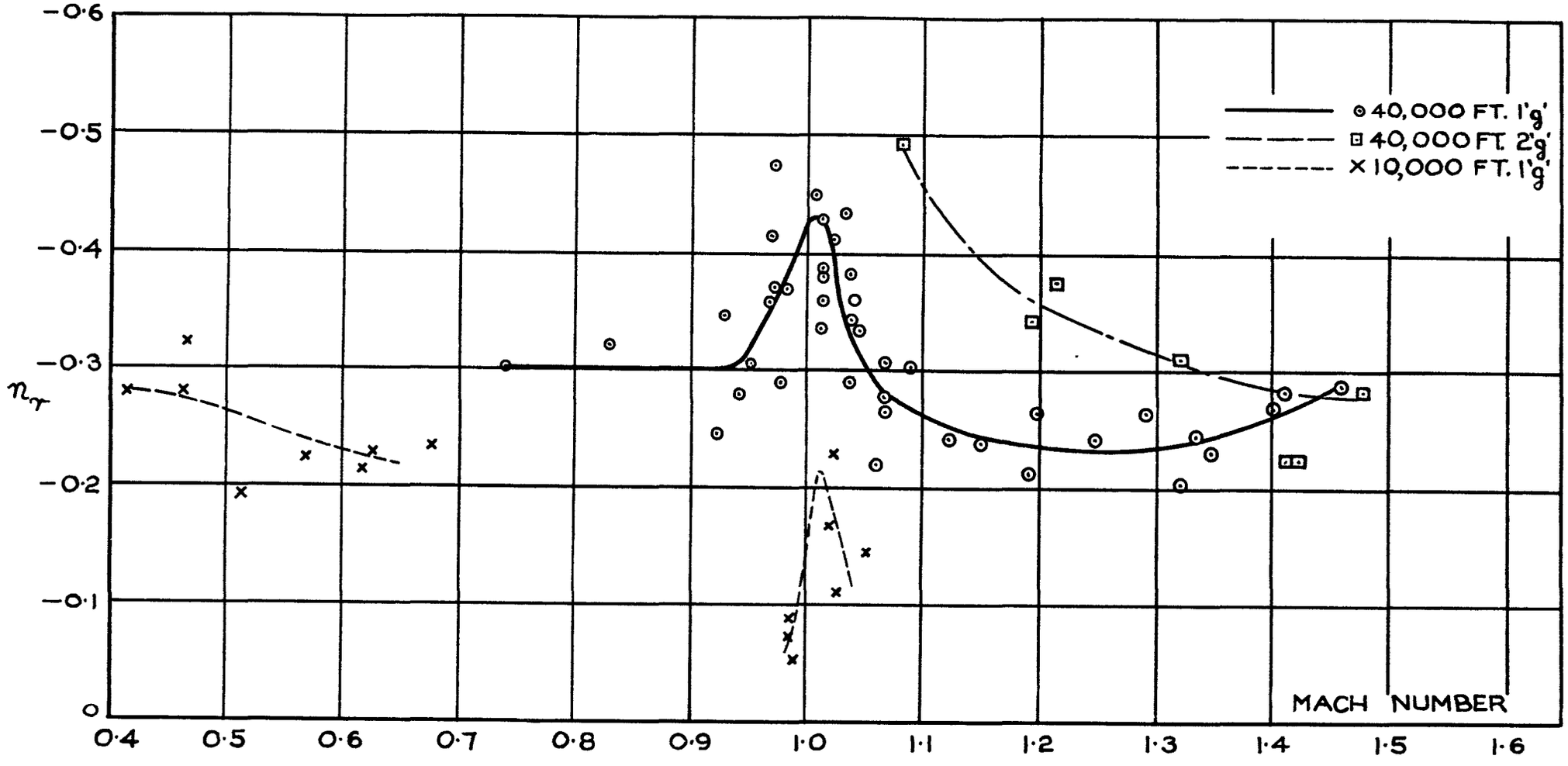

FIG. 34. VARIATION OF THE DAMPING IN YAW DERIVATIVE n_r WITH MACH NUMBER BY VECTOR ANALYSIS.
FAIREY DELTA 2.

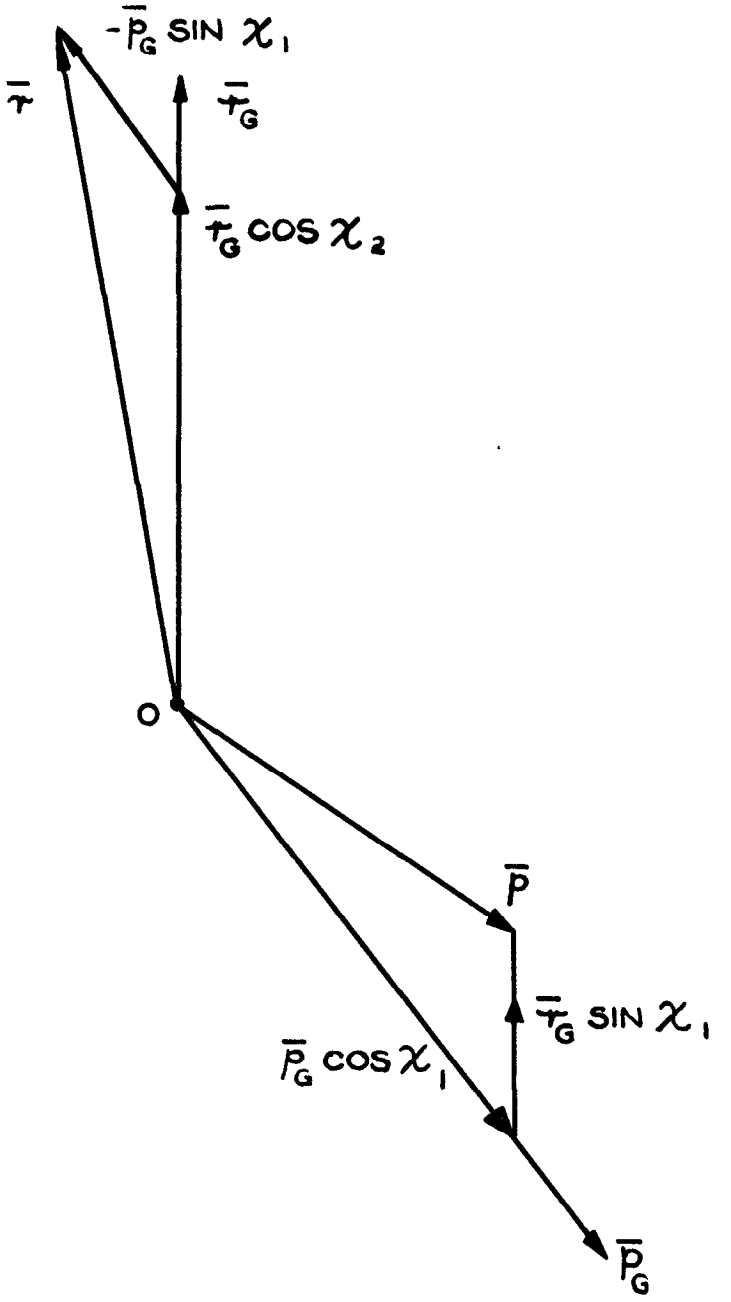

FIG. 35. TRANSFORMATION OF RATES OF ROLL AND YAW TO STABILITY AXES BY TIME VECTOR METHOD.

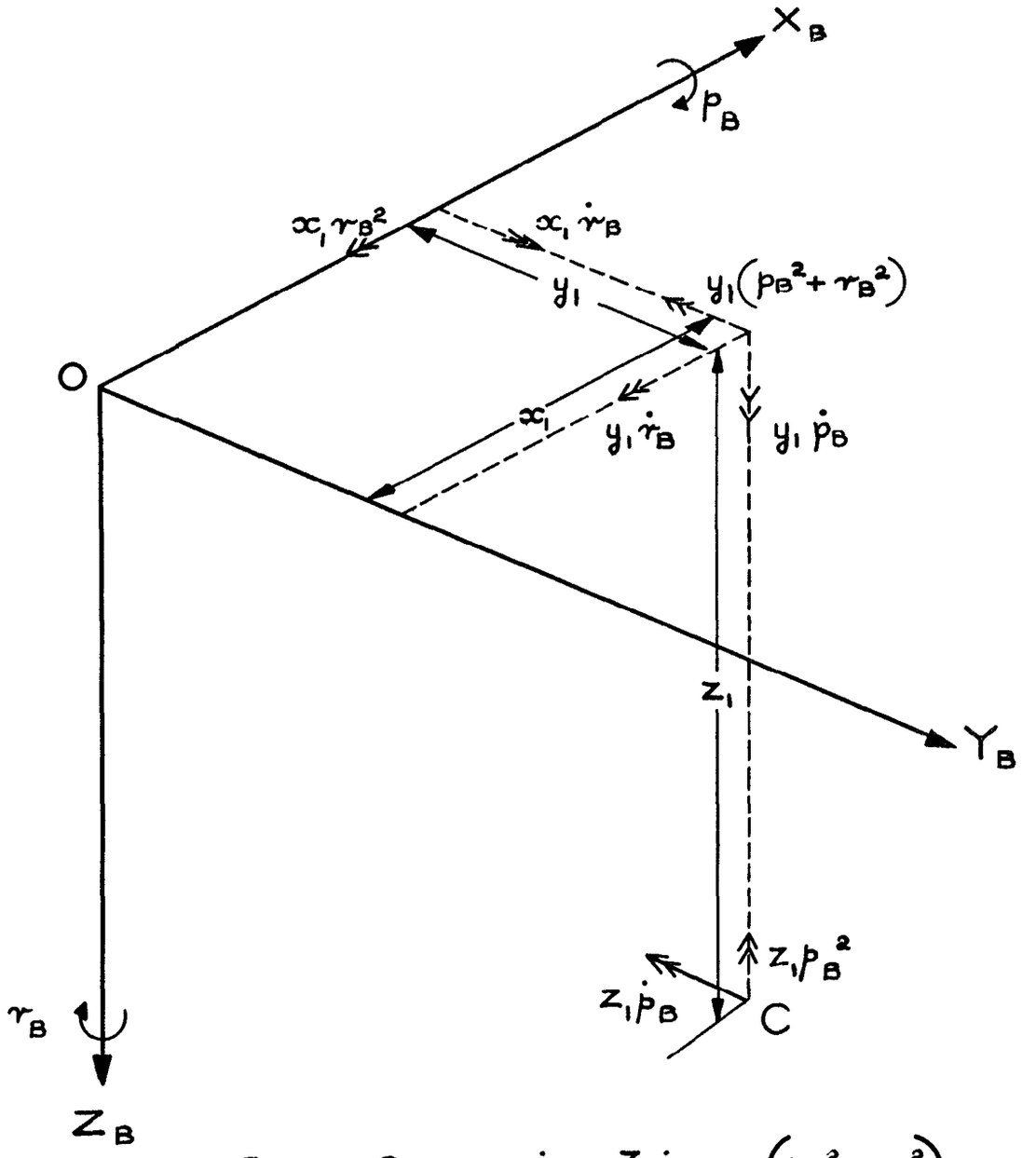

$$a_{y_l} = a_y + x_1 \dot{r}_B - Z_1 \dot{p}_B - y_1 (p_B^2 + r_B^2)$$

FIG. 36. BODY DATUM AXES SHOWING RELATIVE ACCELERATIONS AT THE LATERAL ACCELEROMETER POSITION.

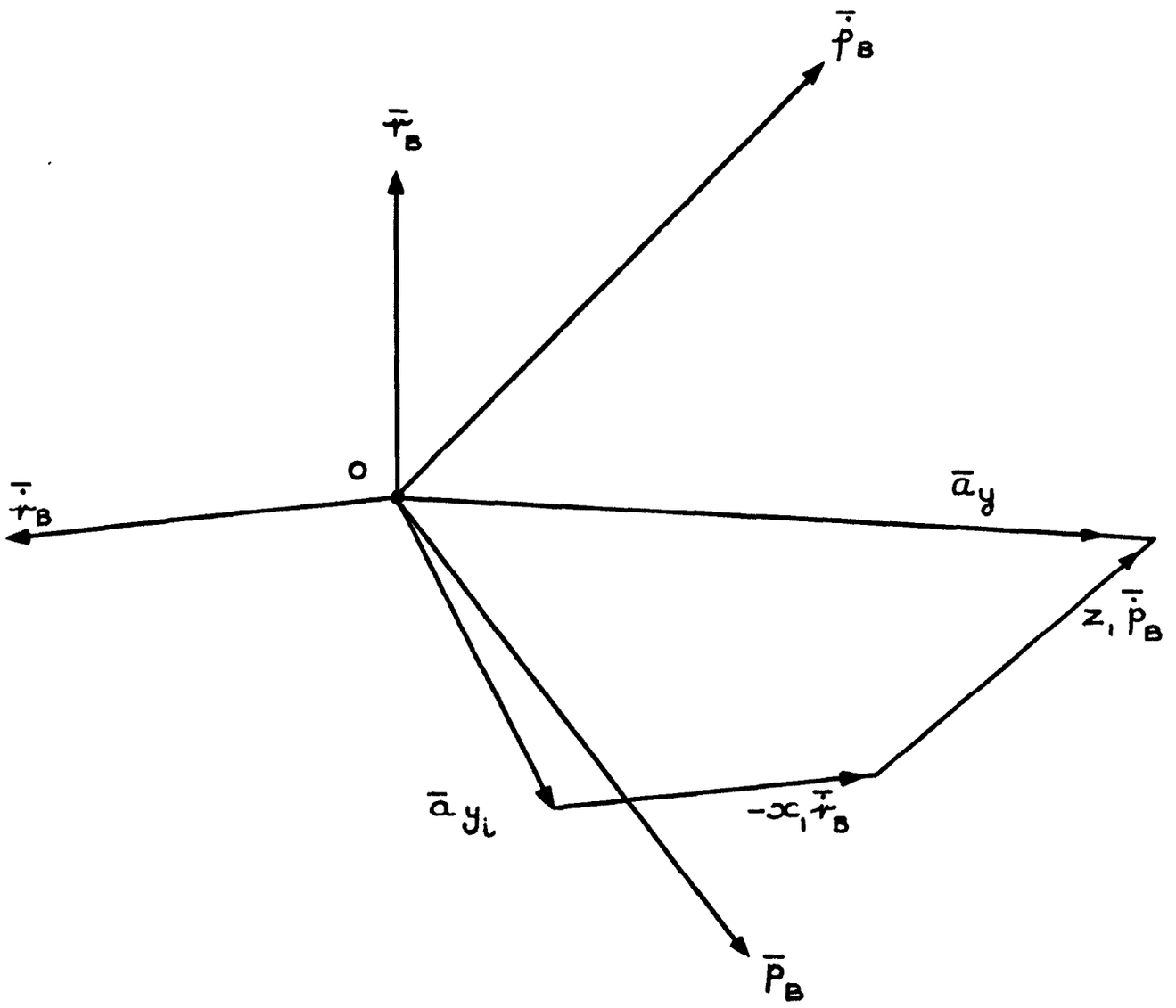

FIG. 37 TRANSFORMATION OF MEASURED VALUES OF LATERAL ACCELERATION TO THE AIRCRAFT CENTRE OF GRAVITY.

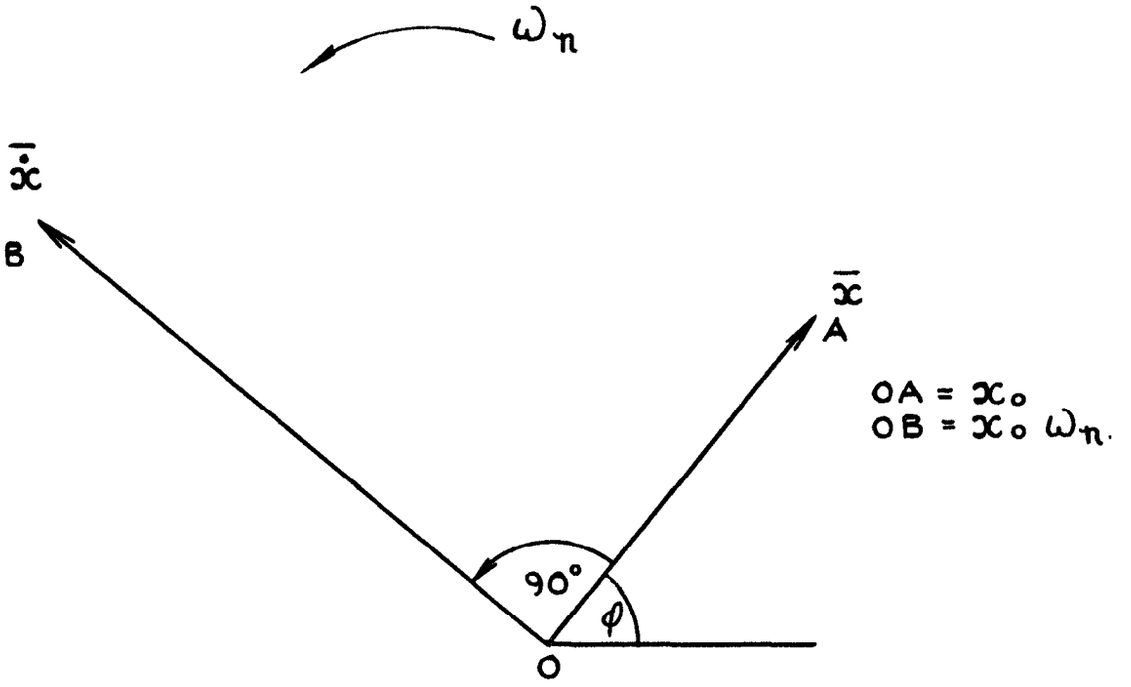

FIG. 38. TIME VECTOR REPRESENTATION OF A SIMPLE SINUSOIDAL OSCILLATION.

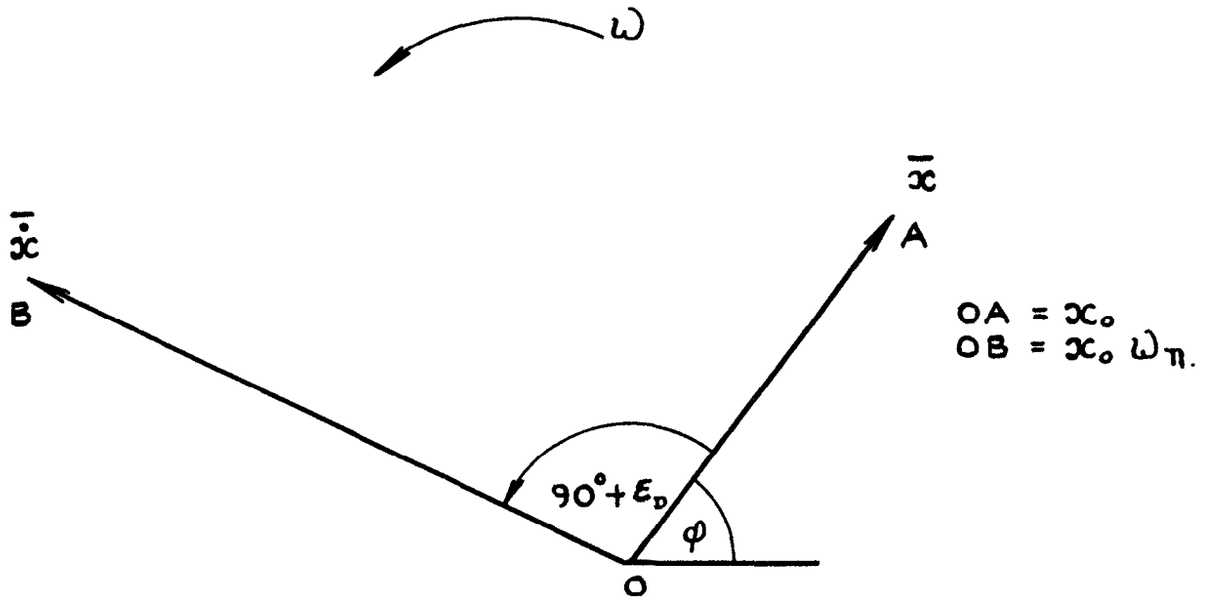

FIG. 39. TIME VECTOR REPRESENTATION OF A DAMPED SINUSOIDAL OSCILLATION.

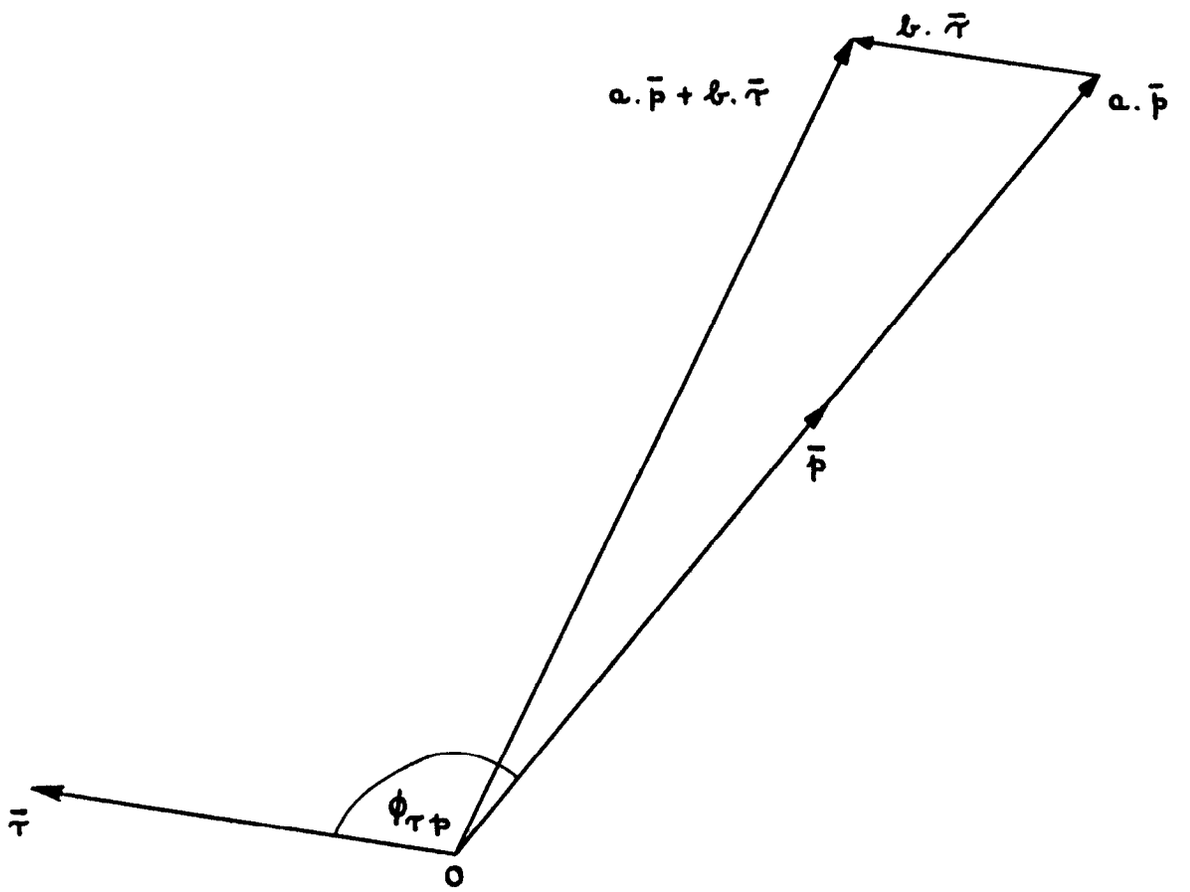

FIG. 40. ADDITION OF TIME VECTORS.

A.R.C. C.P. No. 653 — 533.652.1: 533.693.3:

FLIGHT MEASUREMENTS OF THE DUTCH ROLL CHARACTERISTICS OF A 60 DEGREE DELTA WING AIRCRAFT (FAIREY DELTA 2) AT MACH NUMBERS FROM 0.4 TO 1.5 WITH STABILITY DERIVATIVES EXTRACTED BY VECTOR ANALYSIS. Rose, R. March 1961. — 533.6.011.3/5: 533.6.053: 533.6.013.16: 533.6.013.413: 533.6.08

Lateral stability tests have been made on the Fairey Delta 2 research aircraft, studying the aircraft response following a rudder pulse. A description is given of the instrumentation used, and instrument response characteristics are discussed. Records of the damped Dutch roll oscillation (which persists after the initial pulse stage) have been analysed by the time vector method. The sideslip derivatives n_v, ℓ_v and y_v, and the damping derivatives n_r and ℓ_p have been extracted using estimated values of the relatively unimportant cross derivatives n_p and ℓ_r, which, due to the limitations of the instruments used, could

A.R.C. C.P. No. 653 — 533.652.1: 533.693.3:

FLIGHT MEASUREMENTS OF THE DUTCH ROLL CHARACTERISTICS OF A 60 DEGREE DELTA WING AIRCRAFT (FAIREY DELTA 2) AT MACH NUMBERS FROM 0.4 TO 1.5 WITH STABILITY DERIVATIVES EXTRACTED BY VECTOR ANALYSIS. Rose, R. March 1961. — 533.6.011.3/5: 533.6.053: 533.6.013.16: 533.6.013.413: 533.6.08

Lateral stability tests have been made on the Fairey Delta 2 research aircraft, studying the aircraft response following a rudder pulse. A description is given of the instrumentation used, and instrument response characteristics are discussed. Records of the damped Dutch roll oscillation (which persists after the initial pulse stage) have been analysed by the time vector method. The sideslip derivatives n_v, ℓ_v and y_v, and the damping derivatives n_r and ℓ_p have been extracted using estimated values of the relatively unimportant cross derivatives n_p and ℓ_r, which, due to the limitations of the instruments used, could

A.R.C. C.P. No. 653 — 533.652.1: 533.693.3:

FLIGHT MEASUREMENTS OF THE DUTCH ROLL CHARACTERISTICS OF A 60 DEGREE DELTA WING AIRCRAFT (FAIREY DELTA 2) AT MACH NUMBERS FROM 0.4 TO 1.5 WITH STABILITY DERIVATIVES EXTRACTED BY VECTOR ANALYSIS. Rose, R. March 1961. — 533.6.011.3/5: 533.6.053: 533.6.013.16: 533.6.013.413: 533.6.08

Lateral stability tests have been made on the Fairey Delta 2 research aircraft, studying the aircraft response following a rudder pulse. A description is given of the instrumentation used, and instrument response characteristics are discussed. Records of the damped Dutch roll oscillation (which persists after the initial pulse stage) have been analysed by the time vector method. The sideslip derivatives n_v, ℓ_v and y_v, and the damping derivatives n_r and ℓ_p have been extracted using estimated values of the relatively unimportant cross derivatives n_p and ℓ_r, which, due to the limitations of the instruments used, could

not be extracted from the flight records. Values of the sideslip derivatives deduced from approximate formulae have been found to be in good agreement with the results from the time vector analysis for the range of flight conditions investigated.

not be extracted from the flight records. Values of the sideslip derivatives deduced from approximate formulae have been found to be in good agreement with the results from the time vector analysis for the range of flight conditions investigated.

not be extracted from the flight records. Values of the sideslip derivatives deduced from approximate formulae have been found to be in good agreement with the results from the time vector analysis for the range of flight conditions investigated.

Published by
HER MAJESTY'S STATIONERY OFFICE

To be purchased from
York House, Kingsway, London w.c.2
423 Oxford Street, London w.1
13A Castle Street, Edinburgh 2
109 St. Mary Street, Cardiff
39 King Street, Manchester 2
50 Fairfax Street, Bristol 1
35 Smallbrook, Ringway, Birmingham 5
80 Chichester Street, Belfast 1
or through any bookseller

Printed in England

S.O. CODE No. 23-9013-53